Spring August 2014

FUNCTIONAL AND COMPARATIVE MORPHOLOGY OF THE NASAL CAVITY IN PHYLLOSTOMID BATS

Thomas P. Eiting
University of Massachusetts - Amherst

FUNCTIONAL AND COMPARATIVE MORPHOLOGY OF THE NASAL CAVITY IN PHYLLOSTOMID BATS

A Dissertation Presented

By

THOMAS P. EITING

Submitted to the Graduate School of the
University of Massachusetts Amherst in partial fulfillment
of the requirements for the degree of

DOCTOR OF PHILOSOPHY

May 2014

Organismic and Evolutionary Biology

FUNCTIONAL AND COMPARATIVE MORPHOLOGY OF THE NASAL CAVITY

IN PHYLLOSTOMID BATS

A Dissertation Presented

By

THOMAS P. EITING

Approved as to style and content by:

Elizabeth R. Dumont, Chair

Duncan J. Irschick, Member

Sheila N. Patek, Member

J. Blair Perot, Member

Elizabeth R. Dumont, Director
Organismic and Evolutionary Biology

DEDICATION

To my parents, who always encouraged me to chase my dreams

EPIGRAPH

History suggests that the road to a firm research consensus is extraordinarily arduous

-Thomas S. Kuhn

ACKNOWLEDGEMENTS

I thank my advisor, Betsy Dumont, for her patient guidance and sage mentoring during the course of my dissertation. She has provided an enriching intellectual environment, and I owe much of my academic development to her. Thanks to Blair Perot, without whom I could not have completed the substantial biomechanics component to my project. His constant encouragement and good humor kept me energized throughout. Sheila Patek and Duncan Irschick both brought unique conceptual and practical perspectives to my committee, and I greatly appreciate their thoughtful contributions. Finally, though not a part of my committee officially, Tim Smith of Slippery Rock University deserves a special mention. Tim taught me most of the histological techniques that I know, he has been incredibly generous with his time and resources, and perhaps most importantly, he has made major theoretical contributions to my understanding of the mammalian nose and to my dissertation generally. I cannot express enough my appreciation for his help and generosity over the years.

Much of my work involved destructive sampling of fluid-preserved museum specimens. In broad terms I would like to thank the generations of naturalists, field biologists, curators, benefactors, and others who have made such collections possible in one way or another. I have always cherished working in such places, which would not be possible without the forward-looking spirit of so many others. For my dissertation I used specimens from the American Museum of Natural History and from the UMass Natural History Collections. I acknowledge the staff of both of these institutions, and in particular I thank Kate Doyle of UMass and Nancy Simmons and Eileen Westwig of the AMNH.

Thanks to the many folks who have helped me troubleshoot histological techniques, in particular Stef Krug, Amanda Holley, Elaine Murray, Jill McCutcheon,

and Kunwar Bhatnagar. Nancy Forger helped with microscopy, and both she and Geert De Vries provided generous lab resources and logistical support for the bulk of my histological work. Skye Long and Beth Jakob provided lab space and equipment for paraffin embedding. Nadya Shlykova also helped with microscopy.

For assistance with computer modeling, I owe immense thanks to Dan Pulaski, who has always been generous with his time and expertise. James Hagadorn generously provided access to a CT scanner at Amherst College, and Fettah Kosar facilitated my use of a micro-CT scanner at Harvard. Chris Zusi, Yang Song, and Mike Martell helped me get my bearings with running computational fluid dynamics simulations.

Numerous agencies and institutions have provided funding for my work. A Doctoral Dissertation Improvement Grant from the NSF provided me with resources to carry out work that was far afield from that of my advisor. Other support came from a David J. Klingener scholarship through UMass, the Society for Integrative and Comparative Biology, and the graduate program in Organismic and Evolutionary Biology.

My time in graduate school has been made more enjoyable by many wonderful people along the way. In particular I thank Sharlene Santana, Jul Davis, Jaime Tanner, Teri Orr, Michael Rosario, Chi-Yun Kuo, Casey Gilman, Justin Henningsen, Dana Moseley, Rachel Bolus, Sara Tourscher, Andy Smith, Yifen Lin, Patrick Green, and Moira Concannon. These folks and many others have been stalwart supporters during my tortuous journey. Finally, a great deal of thanks goes to Penny Jaques, for her boundless support and help in navigating the ocean of requirements to get to this point.

ABSTRACT

FUNCTIONAL AND COMPARATIVE MORPHOLOGY OF THE NASAL CAVITY IN PHYLLOSTOMID BATS

MAY 2014

THOMAS P. EITING, B.S., THE UNIVERSITY OF TEXAS AT AUSTIN

M.Sc., UNIVERSITY OF MICHIGAN, ANN ARBOR

Ph.D., UNIVERSITY OF MASSACHUSETTS AMHERST

Directed by: Professor Elizabeth R. Dumont

The functional morphology and evolution of the nasal cavity is poorly understood. The New World Leaf-nosed bats of the family Phyllostomidae are an excellent group of mammals in which to study the evolution of the nose and nasal cavity. Phyllostomids span a wide dietary diversity, which is correlated both with the shape of the rostrum as well as with reliance on olfaction, one of the key functions mediated by the nose and the focus of my dissertation. How does dietary diversity relate to differences in the olfactory anatomy of phyllostomids?

I examined three neurological features thought to relate to olfactory capability, with my hypothesis being that fruit-and nectar-feeding bats rely more on olfaction than insect-feeders. I expected that fruit- and nectar-feeders would have relatively greater numbers of the three neuronal measures that I selected compared to insect-feeders. My results mostly supported this prediction, lending support to the basic idea that bats with different diets rely on olfaction to different degrees.

To sense odors in the environment, incoming air loaded with odorant molecules must make its way to the back of the nasal cavity, where the olfactory epithelium is

located. Do bats with different diets differ in terms of olfactory airflow? In this part of my dissertation, I first performed a computer modeling experiment that tested the hypothesis that the size of the olfactory recess (a key feature of many keen-smelling mammals) relates to differences in important aspects of olfactory airflow. I found that, all else being equal, a larger olfactory recess improves olfactory airflow. Next I performed a comparative study on six species of bats with different diets, expecting to find differences in patterns and rates of olfactory airflow. Instead I found relatively little variation in all of the measured parameters across the species I selected. These results suggest that the morphology of the nasal cavity may not be under strong selective pressure to accommodate different demands on the olfactory system. Investigating this idea more fully, and its consequences for the evolution of the nose and of the skull more broadly, would be an exciting avenue for future research.

TABLE OF CONTENTS

Page

LIST OF TABLES

LIST OF FIGURES

CHAPTER 1

DIET AND ITS RELATIONSHIP TO NEUROANATOMICAL DIFFERENCES IN THE OLFACTORY SYSTEM

1.1 Abstract

Comparative studies are a common way to address large-scale questions in sensory biology. For studies that investigate olfactory abilities, the most commonly used metric is relative olfactory bulb size. Such studies have suggested that fruit- and nectar-feeding bats utilize olfaction more than their insect-eating counterparts. However, recent work has called into question the broad-scale use of relative olfactory bulb size. In this paper I use three neuroanatomical measures with a more mechanistic link to olfactory function (number of olfactory sensory neurons (OSNs), number of mitral cells (MCs), and number of glomeruli) to ask how species with different diets may differ with respect to olfactory ability. I use phyllostomid bats as my study system because behavioral and physiological work has shown that fruit- and nectar-feeding bats rely on odors for detecting, localizing, and assessing potential foods, while insect-eating species do not. Therefore, I predicted that fruit- and nectar-feeding bats would have larger numbers of these three neuroanatomical measures than insect-eating species. In general, my results supported my predictions. I found that fruit-eaters had greater numbers of OSNs and glomeruli than insect-eaters, though I found no difference between groups in number of MCs. Interestingly, nectar-feeders tended to fall in the range of insect-eaters instead of fruit-eaters, though this finding could be the result of only having two nectar-feeders in my analysis. Finally, I examined the relationship between the three neuroanatomical variables and olfactory bulb volume, to determine if olfactory bulb size relates to these

three variables that have a more explicit link with olfactory function. I found that olfactory bulb size was related in an isometric fashion with all three neuroanatomical variables. These findings lend support to the notion that neuroanatomical measures can offer valuable insights into comparative olfactory abilities, and they suggest that the size of the olfactory bulb may be an informative parameter to use at the whole-organism level.

1.2 Introduction

Olfaction plays a critical role in the lives of most mammals. It functions in food detection and discrimination, mother-offspring recognition, species discrimination, and mate choice. Mammals vary in their reliance on olfaction, with cetaceans having little to no olfactory ability and groups like canids relying a great deal on their sense of smell (Anisko, 1976; Pihlström, 2008). Comparative studies have often been used to investigate the evolutionary history of olfactory abilities across mammals. Most comparative studies examine neuroanatomical proxies for olfactory abilities and evaluate their relationship to potential selective pressures (e.g., Baron et al., 1983; Barton et al., 1995; Hutcheon et al., 2002; Barton, 2006). The most common proxy for olfactory ability is the relative size of the olfactory bulb, which has been used in numerous studies of mammals to relate olfactory ability to foraging ecology, activity patterns, and sociality (e.g., Bhatnagar and Kallen, 1974; Gittleman, 1991; Barton et al., 1995; Hutcheon et al., 2002). One group of mammals for which investigations into olfactory function have been extensively studied is phyllostomid bats. This family of bats spans the greatest range of dietary diversity among any mammalian family, having members that consume fruit, nectar, arthropods, vertebrates, and even blood. Comparative studies have shown that bats feeding on fruit

and flowers have relatively larger olfactory bulbs compared to insect-feeders (Bhatnagar and Kallen, 1974; Hutcheon et al., 2002; Safi and Dechmann, 2005), suggesting that these bats use olfaction to different degrees while foraging. Behavioral work has provided further evidence for these ideas, showing that many fruit- and nectar-feeding bats employ olfaction to detect and localize fruit and flower odor sources (Thies et al., 1998; von Helversen et al., 2000; Korine and Kalko, 2005). Physiological work has also shown that fruit-eaters can discriminate ripe fruits at very low odorant thresholds (Laska, 1990). Insect-feeders, by contrast, generally use echolocation and vision when foraging rather than olfaction (Altringham and Fenton, 2003). Olfactory cues are thought to be less informative for these animals, because they hunt moving prey and often catch insects while in flight, and odors are generally too slow-moving to be of much use. Thus both comparative and behavioral work has supported the role for olfactory differences in foraging ecology among bats.

However, a growing body of evidence suggests that the commonly used metric of relative olfactory bulb size may not relate to discernible differences in specific olfactory functions (Laska et al., 2000; Laska et al., 2005; Smith and Bhatnagar, 2004; Joshi et al., 2006; Sarko et al., 2009). Instead, these studies suggest that more direct measures of olfactory performance should be used when possible. For example, Joshi et al. (2006) found that, even though spider monkeys have much smaller relative olfactory brain structures compared to mice, these two species (monkeys and mice) show no appreciable difference in olfactory sensitivity among several odors. However, such physiological comparisons of olfactory performance are limited, because they test only a few odorants

at a time, and they can only be applied to species in captivity or that are easy to study in the field.

The difficulties both of using relative olfactory bulb size and of performing physiological comparisons on multiple species highlight a need to evaluate other metrics for comparative studies. Fortunately, there are several neuroanatomical measures of olfactory reliance (i.e. how much a species depends on olfaction) that have been suggested in the literature. For example, the sheer number of neurons is often taken as an informative measure of computational ability, both across the brain and within more specific regions of the brain (Herculano-Houzel et al., 2006; Herculano-Houzel et al., 2007; Lent et al., 2012; Williams and Herrup, 1988). In the olfactory system, the two sets of neurons that are often investigated are the primary olfactory sensory neurons (OSNs) in the olfactory epithelium, and the mitral cells (MCs), which are the primary neurons within the olfactory bulb (Royet et al., 1998; Schoenfeld and Knott, 2004). Another structure of the olfactory bulb, the glomerulus, has been suggested to be the "functional unit" within the olfactory bulb, and thus could be related to a species' olfactory ability (Allison and Warwick, 1949; Mombaerts et al., 1996; Royet et al., 1998; Cleland and Linster, 2005). Glomeruli are clustered regions of neuropil (regions of high density of axons and dendrites) in the olfactory bulb where the first synapse in olfactory processing occurs (between OSNs and MCs). Each odor seems to evoke responses in a unique set of glomeruli (Mombaerts et al. 1996), so having more glomeruli should allow an animal to distinguish among a larger set of odors.

Using phyllostomid bats I examine how these neuroanatomical measures may be used to study olfactory reliance in a comparative context. Our overarching hypothesis is

that fruit- and nectar-feeding bats rely more on olfactory cues when foraging compared to insect-eating bats. If true, I expect to find that fruit- and nectar-feeders have relatively more OSNs, mitral cells, and glomeruli compared to insect-eaters. I also place our findings in context of the long-established relationship between olfactory bulb size and diet in this group by testing whether the neuroanatomical measures used here relate to olfactory bulb size. Finally, I discuss the implications of our findings for understanding olfactory evolution in this diverse group of mammals.

1.3 Materials and Methods

I sampled adults from 12 species of New World leaf-nosed bats (Family Phyllostomidae). The species that I included consume either fruit, nectar, or insects (see Appendix 1; (Ferrarezzi and Gimenez, 1996; Dumont et al., 2012). All specimens were preserved in 70% ethanol in museum fluid collections (see Appendix 1). I removed the heads, decalcified them using a formic acid-sodium citrate solution, and tested for decalcification using an ammonium oxalate solution. Decalcification took between nine and 30 days, with larger specimens requiring more time. After decalcification, bats were dehydrated through a graded series of alcohol, cleared using Xylene or Histoclear (National Diagnostics), and embedded in Paraplast X-TRA (Fisher Scientific). Specimens were sectioned in the coronal plane rostrally to caudally at nominally 10 µm increments on a rotary microtome (American Optical at UMass or Microm HM 315 at SRU). Every 5^{th} section was mounted on a glass slide until the end of the olfactory epithelium was reached; from this point back to the choana, every 10^{th} section was mounted. Sections were stained with hematoxylin and eosin. Intervening sections were mounted to

supplement the initial sampling as needed and stained with Gomori trichrome or thionine. Slides were cover-slipped with Permount in preparation for microscopic examination.

Microscopic analysis was performed on a light microscope (Eclipse E600, Nikon) with an automated stage (Biopoint 2, Ludl Electronic Products) and digital video camera (Optronics) attached to a computer. The nasal cavity, skeleton, and olfactory bulbs are approximately symmetric about the mid-sagittal plane, so I analyzed only the right side of these structures. For each sample I identified the first and last sections that contained any of the relevant tissue (i.e. olfactory epithelium, if looking at the nasal cavity, or the glomerular and mitral cell layers, if looking at the olfactory bulb). Olfactory epithelium (OE) is readily distinguished from other epithelial types lining the nasal cavity by a combination of traits, including its association with Bowman's glands, the presence of non-motile cilia rather than kinocilia at the apical end, and a clear separation into three cell layers (Fig. 1.1). Supporting cells occupy the apical-most cell layer, and they are usually slightly larger and more oval in shape than the round sensory cells beneath them. Basal cells occupy the basal-most layer (immediately above the lamina propria), and they usually have irregular or flat shapes. For this study I considered all cells between the apical-most and basal-most layers as OSNs (i.e., excluding the supporting and basal cells themselves), and only counted these cells. Some work has suggested that counting dendritic knobs provides a good metric for counting functional OSNs (Farbman, 1992; Schoenfeld and Knott, 2004). However, our sections were relatively thick for this purpose. Although I may have somewhat overestimated the number of functional OSNs (as opposed to new OSNs that have yet to establish a synapse), this has been done consistently across the samples. By studying all OSNs, I assume a similar rate of synapse

formation across species. In the olfactory bulb, glomeruli are large bundles of neuropil at the periphery of the bulb and are easily identified (Fig. 1.2). Mitral cells lie deep to the glomeruli, occurring in a distinct mitral cell layer (MCL) between the external plexiform layer and the internal plexiform layer. Within the MCL mitral cells were easily distinguished from glial cells by their large size, light-staining nucleus, and presence of at least one dark-staining nucleolus (Price and Powell, 1970).

I carried out stereology using StereoInvestigator software (MBF Bioscience, Williston, VT, USA) and estimated the numbers of OSNs in the olfactory epithelium and mitral cells in the olfactory bulb using the optical fractionator technique (West et al., 1991; Mouton, 2011). After determining the first and last sections that contained the structure of interest, I selected eight-to-12 intervening sections in a systematic-random fashion (i.e. random starting section with evenly-spaced sections thereafter) for stereological analysis (Gundersen and Jensen, 1987; Gundersen et al., 1999; Mouton, 2011). I traced the outline of the olfactory epithelium or mitral cell layer in each slice at 40x magnification using a Wacom computer screen that showed a live feed from the video camera. I next overlaid a randomly-oriented virtual grid to select sites at which cells (in the case of OSNs) or cell nuclei (in the case of mitral cells) would be counted at 1000x with an optical disector probe. An optical disector probe is a virtual square box of known dimensions that is used to include or exclude cells with which it comes into contact. We excluded all cells that contacted three of the six planes of the probe (lower z-axis, left y-axis, bottom x-axis) from our counts, and I only included cells if they came into focus within the disector probe. For the olfactory epithelium, I used an optical disector probe of 10 µm x 10 µm and a grid spacing of 100 µm x 100 µm, 125µm x

125µm, or 150µm x 150µm, depending on species. For the mitral cell layer, I used an optical disector probe of 25 µm x 25 µm or 40 µm x 40 µm and a grid spacing of 50 µm x 50 µm, 60 µm x 60 µm, or 80 µm x 80 µm. All probes were 7 µm thick, and they all had a guard zone of 0.5 µm at the top (z-axis), to compensate for shearing effects caused by the microtome. To calculate the total number of OSNs, I multiplied the number of OSNs I counted by the inverse of the section sampling fraction, area sampling fraction, and thickness sampling fraction (Mouton, 2011). Probe dimensions, grid spacing, and inter-section sampling rate were chosen to yield an estimated coefficient of error per specimen of less than 10%, calculated according to the revised quadratic approximation formula with a smoothness class parameter of one (m = 1; Gundersen et al., 1999).

I counted glomeruli using a combination of the physical disector probe and fractionator sampling. I determined the first and last sections that contained glomeruli. I again used systematic-random sampling to choose eight-to-12 sections through the glomerular region. For each of these "reference" sections, I outlined the glomerular layer and each individual glomerulus on the computer screen. I then chose the next section in sequence (separated by 50 µm) and lined up its glomerular layer with the tracing from the reference section. Glomeruli on the second section were marked if they did *not* overlap with the glomerular tracings from the reference section. The number of glomeruli that I counted was then multiplied by the ratio of sampled sections to total sections, giving the total number of glomeruli for the specimen.

My histologically-prepared samples resulted in differential shrinkage of the brains (including the olfactory bulbs) across species, so I was unable to use volumes of the brain or olfactory bulb from my prepared specimens. Instead, I collected values for olfactory

bulb volume and brain volume from the literature (see Appendix 1; (Baron et al., 1996). Baron et al. (1996) extracted brains from fresh-caught specimens, which were immediately fixed in Bouin's solution. This protocol ensured minimum shrinkage, and subsequent measurements by these authors corrected for volumetric loss due to fixation (for further details, see Baron et al., 1996).

All statistical analyses accounted for phylogenetic relationships between species. I used Phylogenetic Generalized Least Squares (PGLS) in my analyses. First I tested for phylogenetic signal in my data (λ; Pagel, 1999). I found that λ differed significantly from 0 but not from 1 in any of my variables, so I assumed Brownian motion in my PGLS models. In my first set of analyses, I examined whether dietary differences (categorical with 3 levels: Fruit, Insects, and Nectar) predict differences in three neuroanatomical variables (continuous; log OSN number, log mitral cell number, and log glomeruli number), with log brain volume as a covariate in each case. Second, I studied the relationship between log olfactory bulb (OB) volume (mm^3) and my three log-transformed neuronal variables by PGLS. In each case, the neuronal measure was the independent variable, and log OB volume was the dependent variable. All statistics were done in R 2.15.1 using the packages "ape," "geiger," "ade4," and "phylosig" (Paradis et al., 2004; Harmon et al., 2008; Revell, 2010; R Core Team, 2012). All of my variables had a lambda value that differed significantly from 0 but not from 1, so I assumed Brownian motion in regression analyses.

1.4 Results

In my first set of analyses I examined the relationship between diet and three variables of functional interest: log OSN number, log mitral cell number, and log glomeruli number, with log brain volume a covariate in each case. I found that diet predicted differences both in log OSN number and log glomeruli number, but not for log mitral cell number (Table 1.1). In the case of log OSN number and log glomeruli number, the difference between the fruit-eating group and the other two dietary groups is driving the overall statistical significance (Fig. 1.3).

I also investigated how my three neuroanatomical variables (numbers of OSNs, mitral cells, and glomeruli) related to olfactory bulb volume. I used PGLS to analyze one each of my three predictor variables (log OSN number, log glomeruli number, and log mitral cell number) against log OB volume. All three variables significantly predicted log OB volume, and the confidence intervals in each case included 1, denoting isometry (Table 1.2; Fig. 1.4).

1.5 Discussion

I found that fruit-eating phyllostomid bats have relatively more olfactory sensory neurons and more glomeruli than their insect-eating counterparts. However, they do not have more mitral cells compared to insect-eaters. In all three analyses nectar-feeders tended to fall in line with the insect-eaters more than the fruit-eaters, though with only two nectar-feeding species in my study it is difficult to make a more general statement with this trend.

These findings thus corroborate the idea that bats with different diets rely on olfaction to varying degrees when foraging. Fruit-eating bats use olfaction for a host of foraging behaviors, including initially detecting fruit odors, following odor plumes, and distinguishing ripe from unripe fruits (Thies et al., 1998; von Helversen et al., 2000; Korine and Kalko, 2005). My work suggests that behavioral differences between these dietary groups may not be the only functionally relevant difference. Indeed, fruit-eating phyllostomids likely have an increased processing capability in their olfactory system for handling food odor cues. Therefore, there seem to be a confluence of behavioral, physiological, and neuronal factors that contribute to the ability of fruit-eating bats to utilize odors in foraging.

Surprisingly, I did not find a relationship between diet and the number of mitral cells. This finding could be due to the fact that mitral cells are not the only cell in the olfactory bulb responsible for transmitting signals. Other neurons, such as tufted cells, and various types of glia interact to form a dense network of connections within the olfactory bulb (Shepherd, 2003). Furthermore, odor processing involves a series of retrograde synapses, lateral inhibitors, and other modifying effects in addition to the routine downstream synaptic connections (Firestein, 2001). Thus it may be profitable to incorporate additional cell types and/or synaptic complexity when investigating comparative olfactory function.

As mentioned, the fact that I only had two nectar-feeders in my study limits my ability to make conclusive general statements. However, it is intriguing to note that these species tend to group with insect-eaters in every analysis. Though other comparative studies have shown that these animals to have relatively large olfactory bulbs, behavioral

studies have found that many nectar-feeders rely on vision and especially echolocation while foraging (von Helversen and von Helversen, 2003; von Helversen and Voigt, 2002). More study, both behavioral and comparative, is clearly warranted.

All three of the neuronal measures I used were related in an isometric fashion to olfactory bulb size. To the extent that my neuronal measures track olfactory functions, these results suggest that relative olfactory bulb size relates to at least some aspects of functional ability. My findings thus support the view that using olfactory bulb size as a proxy for olfactory ability or reliance is a reasonable generalization in comparative studies (Barton, 2006; Barton et al., 1995; Healy and Guilford, 1990). However, the value of using olfactory bulb size in this way is still up for debate. In a comparative neuroanatomical study of five insectivores, Sarko et al. (2009) found that olfactory bulb size increases more slowly than its number of neurons, thereby suggesting that olfactory bulb size should not be used as a proxy for neuron number. However, Sarko et al. (2009) did not include confidence intervals for the estimate of their scaling parameter, so a difference from isometry was not directly tested. Other work questioning the use of olfactory bulb size as a proxy for ability comes from physiological studies. These studies find that olfactory bulb size does not relate to differences between species in terms of the threshold response to various odors, or to discrimination between different odors (Laska et al., 2000; Laska et al., 2005; Hepper and Wells, 2012; Rizvanovic et al., 2013). Such studies are harder to make sense of, but they do point to the need for additional work that uses olfactory bulb size directly as an independent variable in physiological studies. Additionally, the importance of differences in olfactory bulb size may relate more to

whole-organism olfactory performance rather than being a predictor of specific differences in, for example, threshold responses to odorants.

My work highlights the need to continue investigating the assumptions underlying comparative olfactory research. To continue doing broad comparative studies, it is important to identify variables that are likely to be related to any of the numerous olfactory abilities. For example, perhaps the size of the olfactory genome relates to the diversity of odors that can be perceived. Larger numbers of olfactory genes presumably correspond to a more diverse array of olfactory receptor proteins in the olfactory epithelium. This, in turn, could increase the diversity of odors that could be sensed. Physiological work has shown that larger total number of olfactory receptor genes relates to an increase in a species ability to distinguish among structurally related odorants (Laska and Shepherd, 2007). Broad-scale studies have illustrated that different families of olfactory genes are linked with large differences in habitat types across mammals (Hayden et al., 2010), suggesting a role for different odors in niche specialization.

1.6 Conclusions

Fruit-eating phyllostomid bats have greater numbers of olfactory sensory neurons and olfactory bulb glomeruli than do insect-eating phyllostomids, suggesting that fruit-eating species may use olfaction in foraging more than their insect-eating counterparts. These neuronal measures also relate to olfactory bulb size in an isometric fashion, lending support to the idea that the olfactory bulb may be a valuable proxy for whole-organism olfactory ability or reliance. Further comparative, physiological, and behavioral studies are needed to understand how neuroanatomical proxies for olfactory reliance

relate to behavioral or perceptual differences in olfactory performance. The three neuronal measures used here may prove to be fruitful variables for future research in comparative studies of olfaction.

Table 1.1 PGLS results of the effect of diet and brain volume on 3 neuroanatomical measures

log OSN number	d.f	*F value*	*p*
diet	2	4.499	**0.0491**
log brain volume (mm^3)	1	29.315	**0.0006**
log MC number			
diet	2	0.893	0.4467
log brain volume (mm^3)	1	3.58	0.0951
log glomeruli number			
diet	2	6.5416	**0.0207**
log brain volume (mm^3)	1	4.0935	0.0777

Table 1.2 PGLS results of the effect of log OSN number, log MC number, and log glomeruli number on log olfactory bulb (OB) volume

Variable	**slope**	**S.E.**	**t**	***p***	**95% C.I.**
log OSN number	0.888	0.1	8.87	<0.001	0.692-1.084
log MC number	1.605	0.653	2.46	0.034	0.326-2.884
log glomeruli number	1.343	0.443	3.03	0.013	0.474-2.212

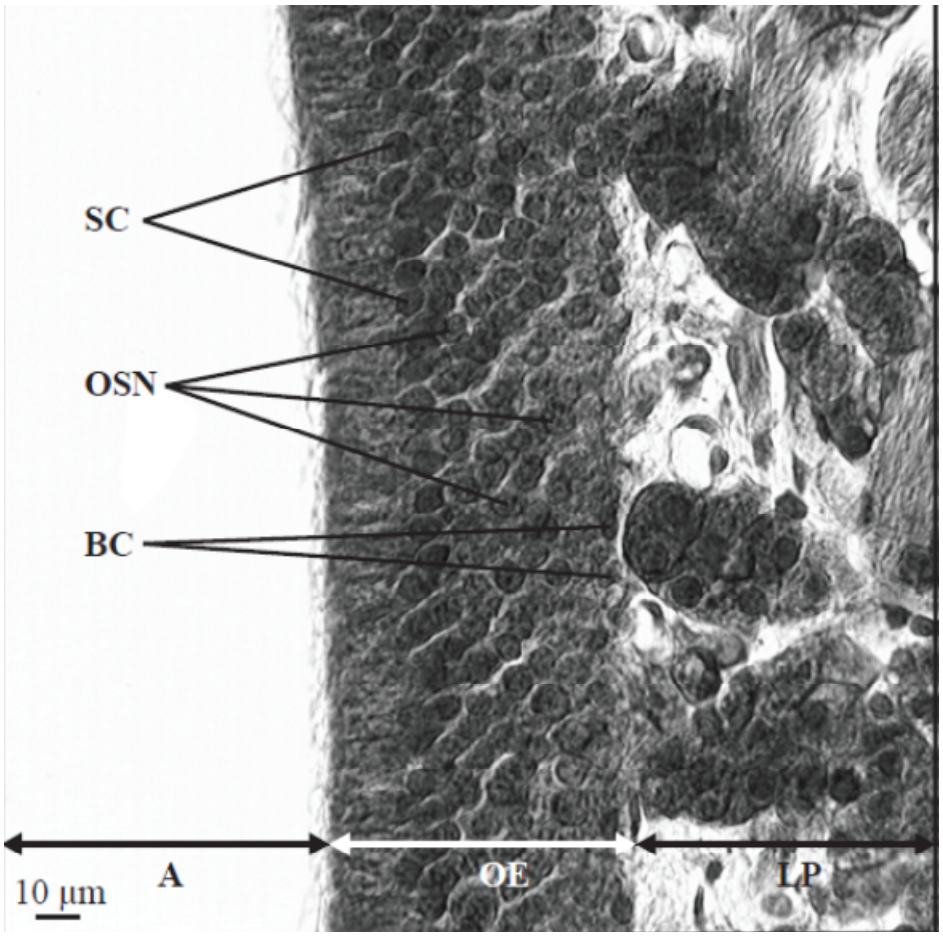

Figure 1.1 Enlarged view of olfactory epithelium (OE). This shows the division of the epithelium into three layers: Supporting Cells (SC), Olfactory Sensory Neurons (OSN), and Basal Cells (BC). Airspace (A) and the underlying lamina propria (LP) shown as reference.

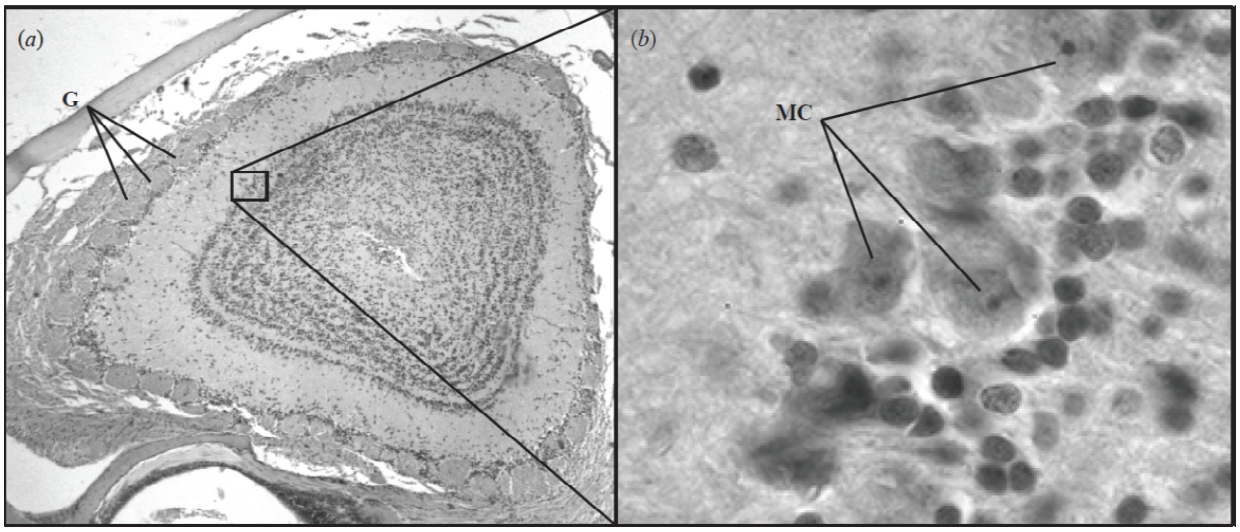

Figure 1.2 Detailed view of the olfactory bulb in *Monophyllus redmani.* (a) Coronal section of the olfactory bulb, showing the glomeruli (G) (40x), (b) High-magnification image of the mitral cell layer in the olfactory bulb, showing the easily-distinguished mitral cells (MC) (1000x).

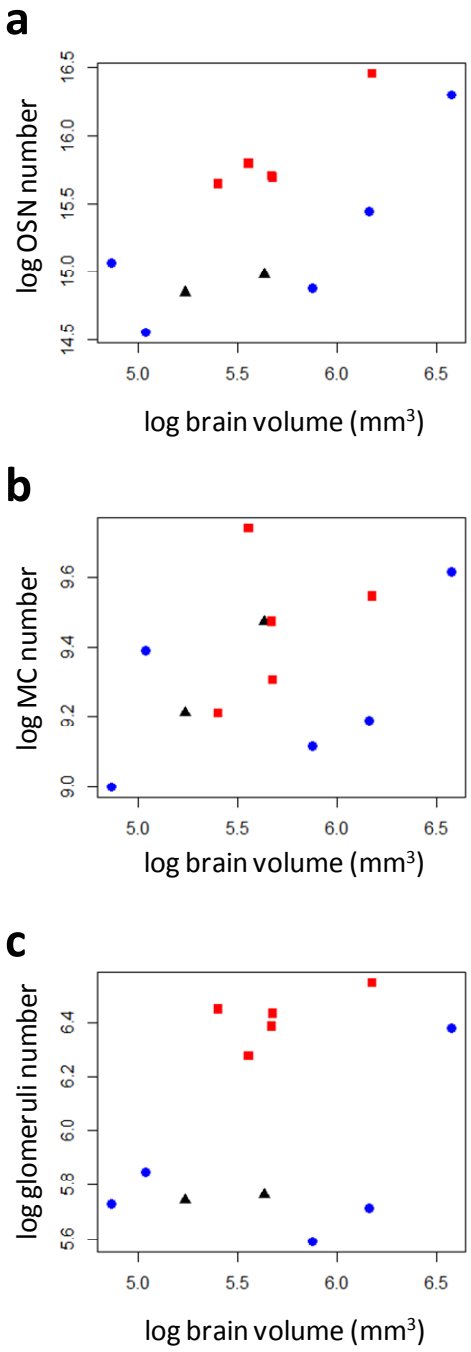

Figure 1.3 Scatterplots of neuroanatomical variables. (a) log olfactory sensory neuron (OSN) number against log brain volume, (b) log mitral cell (MC) number against log brain volume, and (c) log glomeruli number against log brain volume. Diet is indicated by color and shape of symbols: red squares = fruit-eaters, black triangles = nectar-feeders, and blue circles = insect-eaters. Results from PGLS indicate that diet predicts differences in log OSN number and log glomeruli number, but not log MC number, when controlling for brain size.

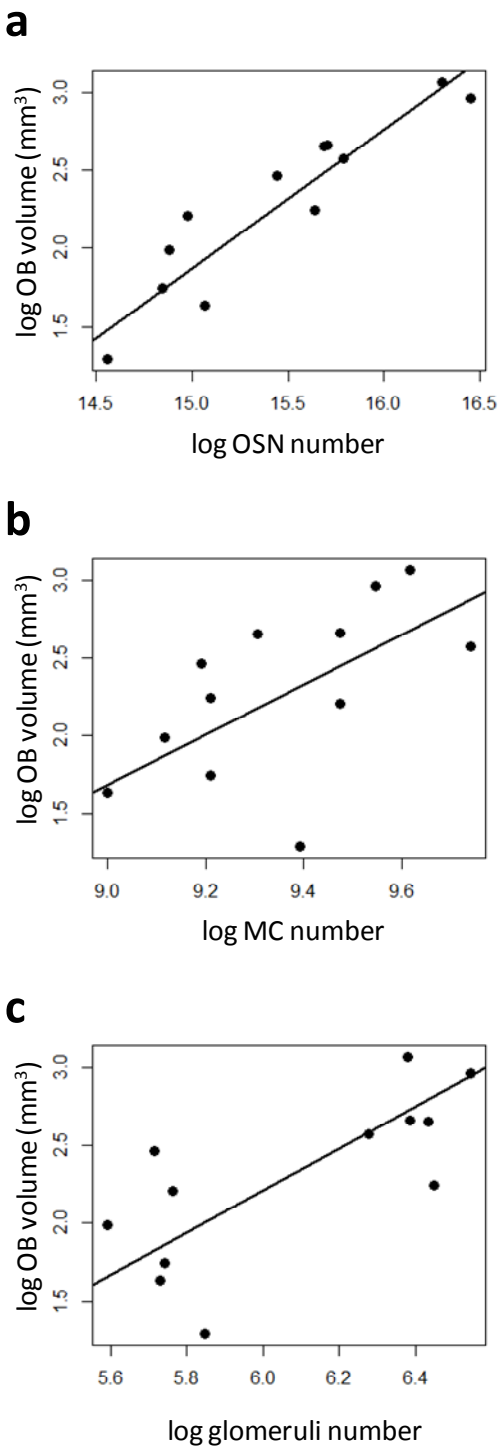

Figure 1.4 Scatterplots of isometric relationships. (a) log olfactory bulb (OB) volume against log olfactory sensory neuron (OSN) number, (b) log OB volume against log mitral cell (MC) number, and (c) log OB volume against log glomeruli number. PGLS indicates that the slope of each line does not differ significantly from 1, thereby indicating isometry (see also Table 1.2).

CHAPTER 2

THE ROLE OF THE OLFACTORY RECESS IN OLFACTORY AIRFLOW

2.1 Abstract

The olfactory recess—a blind pocket at the back of the nasal airway—is thought to play an important role in mammalian olfaction by sequestering air outside of the main airstream, thus giving odorants time to re-circulate. Several studies have shown that species with large olfactory recesses tend to have a well-developed sense of smell. However, no study has investigated how the size of the olfactory recess relates to air circulation near the olfactory epithelium. Here I used a computer model of the nasal cavity from a bat to test the hypothesis that a larger olfactory recess improves olfactory airflow. I predicted that during inhalation, models with an enlarged olfactory recess would have slower rates of flow through the olfactory region (i.e. the olfactory recess plus airspace around the olfactory epithelium), while during exhalation these models would have little to no flow through the olfactory recess. To test these predictions I experimentally modified the size of the olfactory recess while holding the rest of the morphology constant. During inhalation I found that an enlarged olfactory recess resulted in lower rates of flow in the olfactory region. Upon exhalation, air flowed through the olfactory recess at a lower rate in the model with an enlarged olfactory recess. Taken together, these results indicate that an enlarged olfactory recess improves olfactory airflow during both inhalation and exhalation. These findings add to my growing understanding of how the morphology of the nasal cavity may relate to function in this understudied region of the skull.

2.2 Introduction

In mammals thought to have a keen sense of smell (macrosmatic mammals), much of the olfactory epithelium lines a *cul-de-sac* at the back of the nose called the olfactory (Moore, 1981; Smith and Rossie, 2008; Smith et al., in press) or ethmoturbinal recess (Maier, 1993). The olfactory recess has only one opening which allows it to sequester the air that is breathed in during inhalation and prevent it from washing out during exhalation. In this way, odorant-laden air that enters the olfactory recess has more time to circulate in the olfactory region and make contact with odor receptors (Yang et al., 2007). Having a well-developed olfactory recess thus likely improves olfactory performance in macrosmatic mammals (Craven et al., 2010; Yang et al., 2007). The development and extent of the olfactory recess varies considerably across mammals, from completely absent in, for example, hominoids and cetaceans (Moore, 1981; Smith et al., in press), to very large and well-developed in groups like canids (Craven et al., 2007). In this paper I examine the effects of the extent of the olfactory recess on the patterns and rates of olfactory airflow.

The olfactory recess forms as the caudodorsal extension of the nasal fossa and is separated from the ventral nasopharyngeal ducts by a fully-formed transverse lamina. The transverse lamina develops when the lateral walls of the vomer fuse to the medial projection of the lateral nasal wall (Smith and Rossie, 2008) (Fig. 1). The transverse lamina and other structures that bound the olfactory recess derive, in great part, from the mesenchymal condensation known as the pars posterior (De Beer, 1937; Moore, 1981; Smith and Rossie, 2008), so the variation in the development of these structures likely contributes to variation in the size of the olfactory recess across mammals.

One clade of mammals that exhibits substantial variation in the extent of the olfactory recess is the New World leaf-nosed bats (Family Phyllostomidae). One way to quantify this difference is to calculate the percentage of olfactory epithelium contained within the olfactory recess. This parameter relates to the size of the olfactory recess because, in all species examined, virtually all of the olfactory recess is lined with olfactory epithelium. I have found that some species have less than 10% of their total olfactory epithelium located within the olfactory recess, while other species have a third or more of their olfactory epithelium located within the olfactory recess (Eiting et al., in review). In this study I examine the hypothesis that an enlarged olfactory recess improves olfactory airflow in phyllostomid bats. To examine this hypothesis, I generated a steady-state model of airflow through the nasal passage of the short-tailed fruit bat, *Carollia perspicillata* (Linnaeus), and compared it to airflow predicted from models in which I artificially reduced and enlarged the olfactory recess. This species is common throughout much of the New World tropics, and it is often used in experimental and behavioral work, including previous work on olfactory sensitivity and discrimination (Laska, 1990a; Laska, 1990b; Thies et al., 1998). *Carollia* lies near the base of the radiation of frugivores within the phyllostomids, and it is morphologically intermediate between the long-nosed nectar feeding bats and the short- nosed canopy frugivores (Dumont et al., 2012; Freeman, 1988; Freeman, 2000). These two features make this species a well-suited model to study olfactory airflow.

If an enlarged olfactory recess improves olfactory airflow, then at a given volumetric flow rate, I expect nasal passages with an enlarged olfactory recess to have lower rates of flow (i.e. volume of flow per unit time) through the olfactory region during

inhalation, which increases residence time of odorant molecules in the airspace above the olfactory mucosa (Craven et al., 2010; Yang et al., 2007). Long residence time is thought to improve absorption efficiency, meaning that proportionally more odorant molecules are absorbed in the mucus (Lawson et al., 2012). Second, I predict that models with an enlarged olfactory recess will have lower rates of airflow and less total airflow through the olfactory recess during exhalation. Lower rates of flow in the olfactory recess during exhalation would mean that air within the olfactory recess will "wash out" relatively slowly. Furthermore, less air moving through the olfactory recess during exhalation would suggest that proportionately less air is washed out of the olfactory recess with each breath cycle, giving odorants more time in the olfactory recess to be absorbed.

2.3 Materials and Methods

I constructed an anatomically accurate 3D finite volume model of the right nasal airway of an adult fluid-preserved *Carollia perspicillata* (AMNH #261433) from a microCT scan (X-Tek HMX ST 225; 72 kV, 148 μA, voxel size: 2.425 x 10^{-2} mm). I used Mimics v. 15.01 (Materialise, Leuven, Belgium) and Geomagic Studio v. 12.0 (3D Systems, Rock Hill, SC, USA) to create a solid model of the airway from the raw stack of CT image slices. My relatively low energy CT scan allowed me to see the air-mucosa boundary throughout much of the scan. In areas where the mucosa could not reliably be distinguished from the surrounding airspace, I consulted slices from a histological preparation of this same specimen of *Carollia* (see details below), which allowed me to see the olfactory mucosa throughout the specimen. I matched the histology slices with the CT slices from the same locations, allowing me to modify the 3D model as needed. I

artificially elongated the nasopharyngeal meatus (posterior opening of the nasal cavity) of my model by ~1.1 mm, to ensure that the flow during exhalation was fully developed at the back of the airway. The model of the air space included approximately 625,000 4-noded tetrahedral elements. I carried out a sensitivity study with twice the number of tetrahedra and found no appreciable differences in my results, so I used the 625k model in this study. To make the histological preparation of my specimen, the head was removed and decalcified in a solution of formic acid and sodium citrate. The specimen was then embedded in paraffin and sectioned on a rotary microtome at nominally 10 μm thickness in the coronal plane.

I mounted every 5th section and stained most slides with hematoxylin and eosin. Some intervening sections were also mounted and stained with Gomori trichrome or thionine. The histological preparations allowed me to examine the location and extent of the olfactory epithelium. I acquired photomicrographs of the sections and used ImageJ software to outline the olfactory epithelium in every 3rd section. I then calculated the amount of olfactory epithelium section-by-section and the cumulative rostro-caudal percentage of olfactory epithelium for the entire specimen. This process allowed me to calculate that 21.5% of all of the olfactory epithelium was located in the olfactory recess (beginning with the first coronal section with a complete transverse lamina) for this specimen.

I also used histological slides to map the olfactory epithelium onto the 3D models. This was done by creating a surface model (STL file) of the olfactory mucosa in Geomagic Studio based on photomicrographs of the histology slides. Anatomical landmarks in the slides were matched to the same landmarks in the original model of the

airway in Geomagic. Once completed, this new STL file of the olfactory mucosa was imported directly into the flow visualization software (Paraview v. 3.98.1, Kitware, Inc., Clifton Park, New York, USA).

To examine the effects of enlarging or shrinking the olfactory recess, I altered the length of the transverse lamina in the *Carollia* model. By lengthening the transverse lamina, I was able to create a model that had a proportionately larger olfactory recess. Similarly, shortening the transverse lamina produced a proportionately smaller olfactory recess. I altered the length of the transverse lamina in the model so that it enclosed an olfactory recess that contained the extremes of variation seen among phyllostomids (i.e. ~7.5% and ~34% olfactory epithelium within the olfactory recess; Fig. 2.1). These alterations were performed by artificially shortening and lengthening the transverse lamina using the modeling software (Geomagic Studio and Mimics).

I assessed steadiness in flow by calculating the Womersley number, which is a value used to distinguish steady from unsteady flow in fluids (Loudon and Tordesillas, 1998). For my study the Womersley number was less than one (0.38), meaning that I could assume steady flow. The Reynolds number for the nasal airway of *Carollia* is on the order of ~20, so I also assumed laminar flow. I applied the same volumetric flow rate to the models during both inhalation and exhalation. The flow rate was determined to be 2.255×10^{-2} L/min, based on the allometric equation suggested by Craven et al. (2010):

$$Q_{peak} = 1.43M^{1.04}, \quad (1)$$

where Q_{peak} is peak inspiratory flow rate, and M is the body mass (in grams). For my models, I used a value of 18.5 for M, which is the average body mass of male *C. perspicillata* in grams (Cloutier and Thomas, 1992). To apply this flow rate at the inlet (i.e. at the nostril during inhalation or at the choana during exhalation), I converted volumetric flow rate into fluid velocity assuming a constant inflow velocity, using the following equation:

$$U = Q/A, \quad (2)$$

where U is the fluid velocity (in m/s), and A is the area of the inlet normal to the direction of low. I used OpenFOAM 1.6-ext (www.openfoam.org) to solve steady-state solutions of inhalation and exhalation (see Appendix B for further details). In the presented simulations the velocity is 0.78 m/s during inhalation, and 0.29 m/s during exhalation. I applied a zero velocity gradient, constant pressure boundary at the outlet (i.e. at the choana during inhalation or at the nostril during exhalation).

My quantitative analyses were performed as follows. For my inhalation case I defined an identical subvolume in all three models that roughly matched the location of the olfactory epithelium (Fig. 2.2). For every cell in this subvolume, I extracted values for velocity magnitude, which were then used to calculate average airflow velocity. These average values were compared across the three models. I also calculated volumetric flow rate. First I selected an identical transverse slice in all three models that corresponded to the anterior-most beginning of the transverse lamina in the reduced olfactory recess model. Then I integrated flow velocity across the area of this slice to calculate volumetric

flow rate. I calculated volumetric flow rate for the exhalation case in the same manner and across the same slice. I also performed qualitative comparisons of flow passing through the olfactory recess by comparing flow patterns using streamlines (i.e. lines of flow tangential to the direction of flow). The streamlines were generated by "seeding" a sphere (radius 0.35 mm) of 500 points near the choana.

2.4 Results

Flow patterns in my computational models for the case of inhaled air support the prediction that a reduced olfactory recess produces higher flow velocities in the olfactory region (Fig. 2.3). I found that airflow in the reduced olfactory recess subvolume was 28% faster on average than in the normal olfactory recess subvolume (11.56×10^{-3} m/s vs. 9.06×10^{-3} m/s). Similarly, airflow in the normal olfactory recess subvolume was an average of 17% faster than in the enlarged olfactory recess subvolume (9.06×10^{-3} m/s vs. 7.74×10^{-3} m/s). When comparing the reduced olfactory recess vs. the enlarged olfactory recess subvolumes, the average flow in the reduced olfactory recess subvolume was nearly 50% faster than in the enlarged olfactory recess subvolume (11.56×10^{-3} m/s vs. 7.74×10^{-3} m/s). Higher flow velocities translate to higher rates of flow in these models. This can be seen in the slice shown in Figure 3, which corresponds approximately to the first slice anterior-posterior slice in which the olfactory recess appears. Flow rate into the olfactory recess at the level of the slice in Figure 3 was highest in the reduced olfactory recess model (6.49×10^{-4} L/min), moderate in the normal olfactory recess model (3.46×10^{-4} L/min), and lowest in the enlarged olfactory recess model (1.27×10^{-4} L/min).

Qualitative comparisons between the three models during exhalation show that more streamlines pass through the same coronal anterior-posterior slice in models with a reduced olfactory recess (Fig. 4). For my quantitative comparisons, I calculated average flow rates for air leaving the olfactory recess at the same anterior-posterior slice as in the streamline comparison. Average rates of flow out of the olfactory recess at this slice were highest in the model with the reduced olfactory recess (5.1×10^{-4} L/min), moderate in the model with the normal olfactory recess (2.25×10^{-4} L/min), and lowest in the model with the enlarged olfactory recess (6.6×10^{-5} L/min).

2.5 Discussion

Computational studies of airflow in mammals have established that the olfactory recess is a region of the nasal fossa that is well-suited for olfaction (Craven et al., 2010; Yang et al., 2007; Zhao et al., 2006). A small fraction of air inhaled during breathing/sniffing bypasses the respiratory region of the nose by a dorsal conduit, and then slows down upon entering the convoluted olfactory region, which ends in the blind olfactory recess. This study is the first to modify the size of the olfactory recess in order to understand if and how much of an impact it has on altering olfactory airflow. I have demonstrated that the size of the olfactory recess contributes significantly to the flow patterns and rates of flow through the olfactory region. These results have implications for an improved understanding of the role that morphology plays in nasal airway function. The simulations of inspiratory airflow produced a steady increase in flow rates (which reduces molecule residence times) through the olfactory region in models with progressively reduced olfactory recesses. Comparing the extreme cases, the flow rate

through the olfactory region of these models was approximately 50% higher in the reduced olfactory recess model compared to the enlarged olfactory recess model. These results indirectly support the hypothesis that the size of the olfactory recess, which is determined by the extent of the transverse lamina, can play a significant role in improving residence time of odorants within the olfactory region. This increase in residence time is predicted to produce a greater fractional uptake of odorants from the total mass flow of odorants at the inlet. To further examine odorant absorption in *Carollia*, I would need to perform simulations of nasal odorant deposition.

On exhalation I saw that as the olfactory recess was enlarged (by elongating the transverse lamina), rates of flow declined. Air that is already in the olfactory recess would thus be pushed out slowly, potentially allowing more time for odorant deposition in this region. I also saw progressively fewer streamlines passing through the olfactory recess as it was enlarged. This predicts that less air is washed out of the olfactory recess as the transverse lamina increases in length. This, in turn, would suggest that odorant molecules, on average, have more time to be absorbed into the mucus overlying the olfactory epithelium, and thereby have a greater chance of coming into contact with olfactory receptors. A fully transient simulation would be needed to investigate the interplay between inhalation and exhalation, and the extent to which inhaled airstreams become entrained in the olfactory recess before being washed out by exhaled air currents.

If increasing the size of the olfactory recess improves odorant residence times, what prevents an animal from elongating the transverse lamina so much that the olfactory becomes nearly completely closed off? The explanation is likely multifaceted, encompassing both developmental and functional constraints. The olfactory recess

develops in concert with the rest of the nasal fossa, the midface, and the braincase. As a result, the size, position, and shape of the olfactory recess are probably limited by the developing forebrain, eyes, and dentition (Moore, 1981; Smith and Rossie, 2008; Smith et al., in press). In addition, the respiratory functions of the nasal fossa (e.g. water retention, filtering) depend on having a large surface area over which air currents must pass. All else being equal, an enlarged olfactory recess would decrease the area and volume available for respiration, especially in short-faced species (Van Valkenburgh et al., 2004; Smith et al., in press).

How can my results be understood in light of studies that have shown that increasing flow rate (including sniffing) actually improves olfactory performance, rather than reducing it (e.g. Tucker, 1963; Oka et al., 2009)? These studies reason, quite correctly, that high flow rates imply that more odorant molecules can pass over the olfactory mucosa within a given period of time, thereby enhancing the olfactory system's ability to sense the odors.

The issue is resolved by focusing on the definition of olfactory performance. If the goal is to smell a 'packet' of odor that is highly localized, such as the odor trail of a plant or another bat, then processing more air (with higher flow rates) does not help the performance of the system. High flow rates in this case just add more air that does not contain the signal of interest. However, a low flow rate allows whatever odor exists in that packet of air to have the maximum time to trigger the sensory system. Put another way, the issue is one of temporal or spatial resolution (if the bat or the air is moving). If the odorant is distributed widely so that high flow rates can be assured of continually delivering air with more of the odorant, then a high flow rate might be an effective means

of sampling. However, many odor signals are not distributed evenly or continuously in the environment. A classic study by Mozell et al. (1984) found that for a given volume of inhaled air, increasing the flow rate has a negative influence on the olfactory response. This is because, if the goal is to process a localized "whiff" of odorant, then it is more effective to slow the packet of air down as much as possible and give the system as much time as possible to be activated.

Sniffing likely improves olfactory processing by combining benefits of both high flow rates initially and low or no flow later. The early sniff involves a large flow rate to rapidly access a large volume of air and as may odorant molecules as possible. The later sniff involves a quiescent period where the net flow rate is almost zero, which lets the system have as much time as possible to trigger the olfactory sensory neurons from the packet of air that has just been obtained. Though I simulated airflow at the predicted high-end of inspiratory flow rates, I have yet to simulate sniffing in an unsteady manner, which is required to more accurately capture patterns and rates of flow during a sniff. I hope to carry out such simulations in the future, which will aid in my understanding of how the dynamics of sniffing impact olfactory airflow.

2.6 Conclusions

My study shows that variations in the size of the olfactory recess likely have significant functional consequences in groups that exhibit extensive variation in olfactory recess size, such as bats and primates (Cave, 1973; Moore, 1981; Smith et al., 2011; Smith et al., 2012; Smith et al., in press). This work also adds to the growing body of computational modeling studies that investigate the role of morphology in airway

function. This computational approach allowed me to assess the potential role of just one morphological variable in affecting nasal airflow. I found that relatively minor modifications to the extent of the olfactory recess can have rather dramatic effects on flow patterns and rates through the olfactory recess. How might other aspects of the morphology relate to differences in flow? How do these morphological differences affect other aspects of nasal airway function, such as respiration or echolocation? Developing methods to adequately address these and other similar questions should contribute fundamentally to my understanding of how this complex region of the skull works.

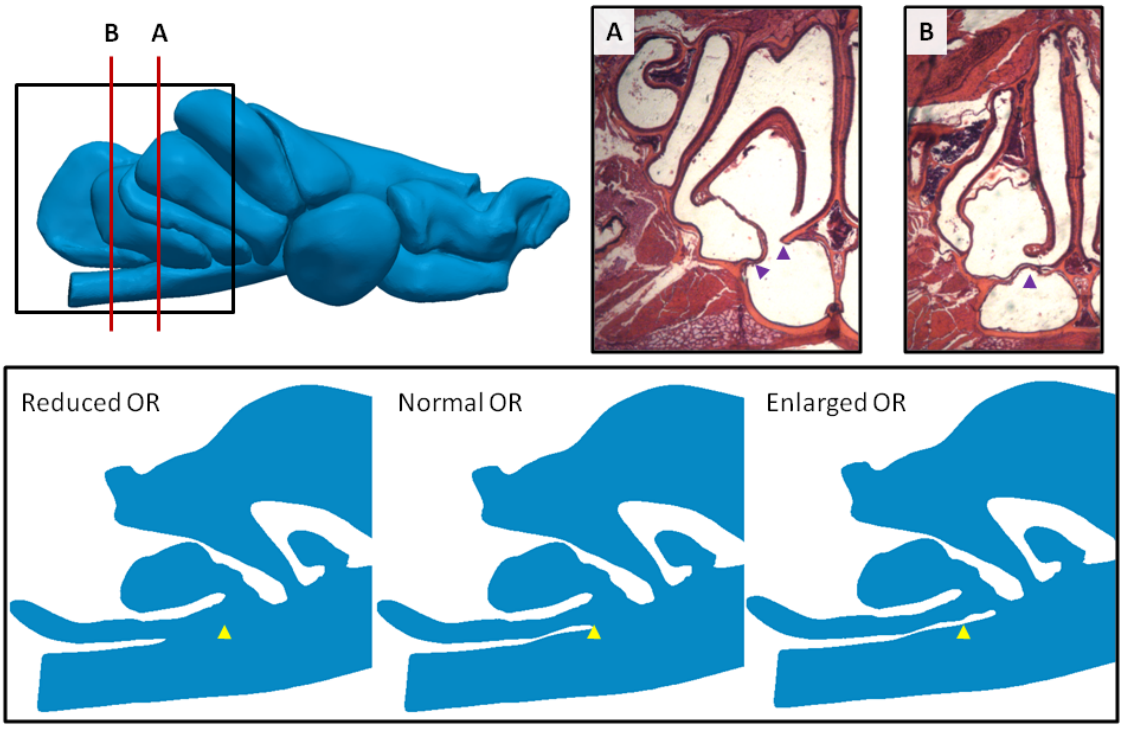

Figure 2.1 Lateral view of right nasal airway, with anterior towards the right. The two red lines correspond to the anterior-posterior location of the two labeled histology slides, which show the formation of the transverse lamina. In "A," the transverse lamina (TL) has not formed, but the lateral extensions of the vomer/nasal septum have nearly reached the medial projection of the lateral wall of the airway (purple arrowheads). In "B," the TL has formed from the merger of the lateral extension of the vomer/septum and the medial extension of the lateral wall (purple arrowhead). The black box surrounding the back ~1/3 of the airway in the top left corresponds to the portion of the model shown in the bottom panel. This bottom panel illustrates the same parasagittal section roughly midway through the airway (i.e. parallel to the plane of the page), with each section coming from one of my three computational models. "Reduced OR" = model with transverse lamina reduced such that only ~7.5% of the total olfactory epithelium lies within the olfactory recess (OR). "Normal OR" = unmodified model of *Carollia perspicillata*, in which 21.5% of olfactory epithelium lies within the olfactory recess. "Enlarged OR" = model with a lengthened transverse lamina such that ~33% of the total amount of olfactory epithelium lies within the olfactory recess. In all three slices, the yellow arrowhead points to the anterior extreme of the TL as found in the "Normal OR" model.

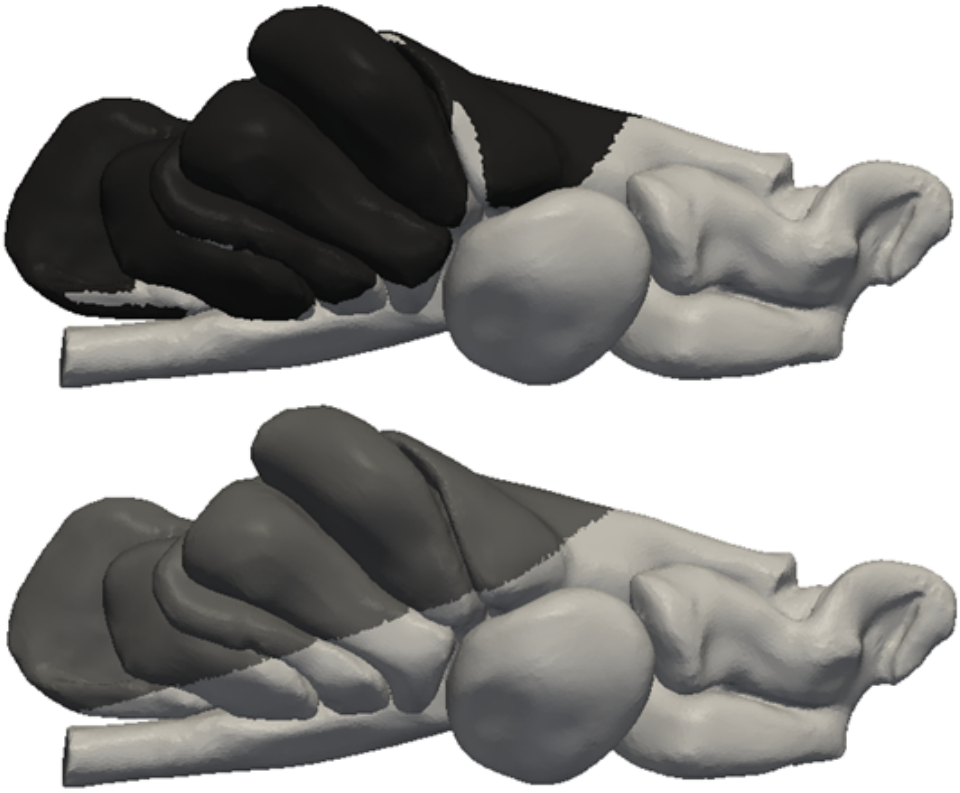

Figure 2.2 Comparison of the location of the olfactory epithelium (black in the top image) with the location of the subvolume used to calculate flow rates during inhalation (gray in the bottom image). Note the approximate overlap between the colored portions of each image. The subvolume in the bottom image was selected based not only on its approximation to the location of the OE, but also on ease and reproducibility of its selection.

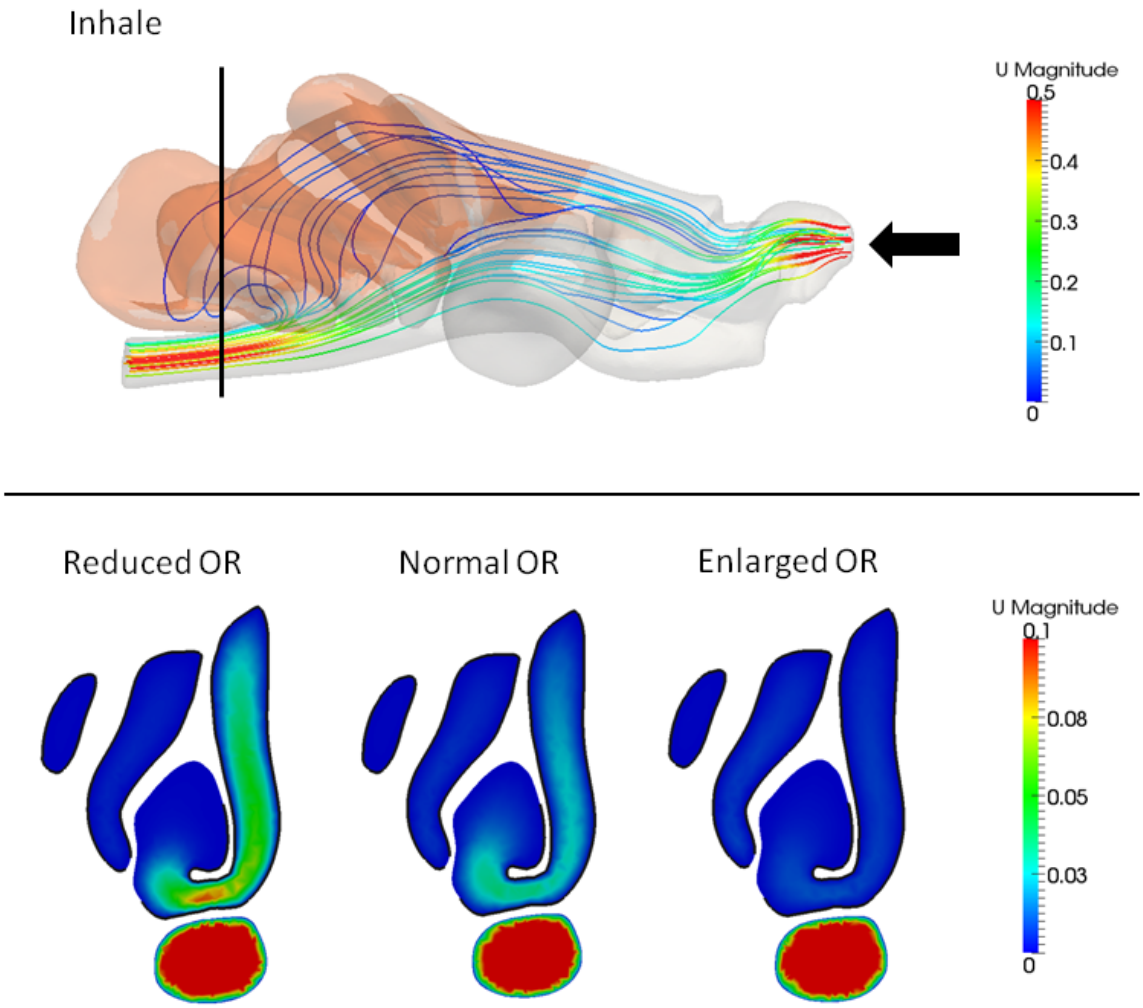

Figure 2.3 Flow rates during inhalation in *Carollia perspicillata*. The top panel shows a lateral view of the whole airway, with anterior towards the right. Flow is in the direction of the black arrow. The location of the olfactory epithelium is shown in orange. Vertical bar shows the location of the first anterior-posterior slice with a complete transverse lamina (i.e. a fully sequestered olfactory recess). This slice forms the basis for comparisons in the bottom panel. "Reduced OR" = model with transverse lamina reduced such that only ~7.5% of the total olfactory epithelium lies within the olfactory recess. "Normal OR" = unmodified model of *Carollia perspicillata*, in which 21.5% of olfactory epithelium lies within the olfactory recess. "Enlarged OR" = model with a lengthened transverse lamina such that ~33% of the total amount of olfactory epithelium lies within the olfactory recess. "U magnitude" refers to the velocity magnitude in m/s. Note the higher flow rates in the reduced OR model, and the lower flow rates in the elongated OR model.

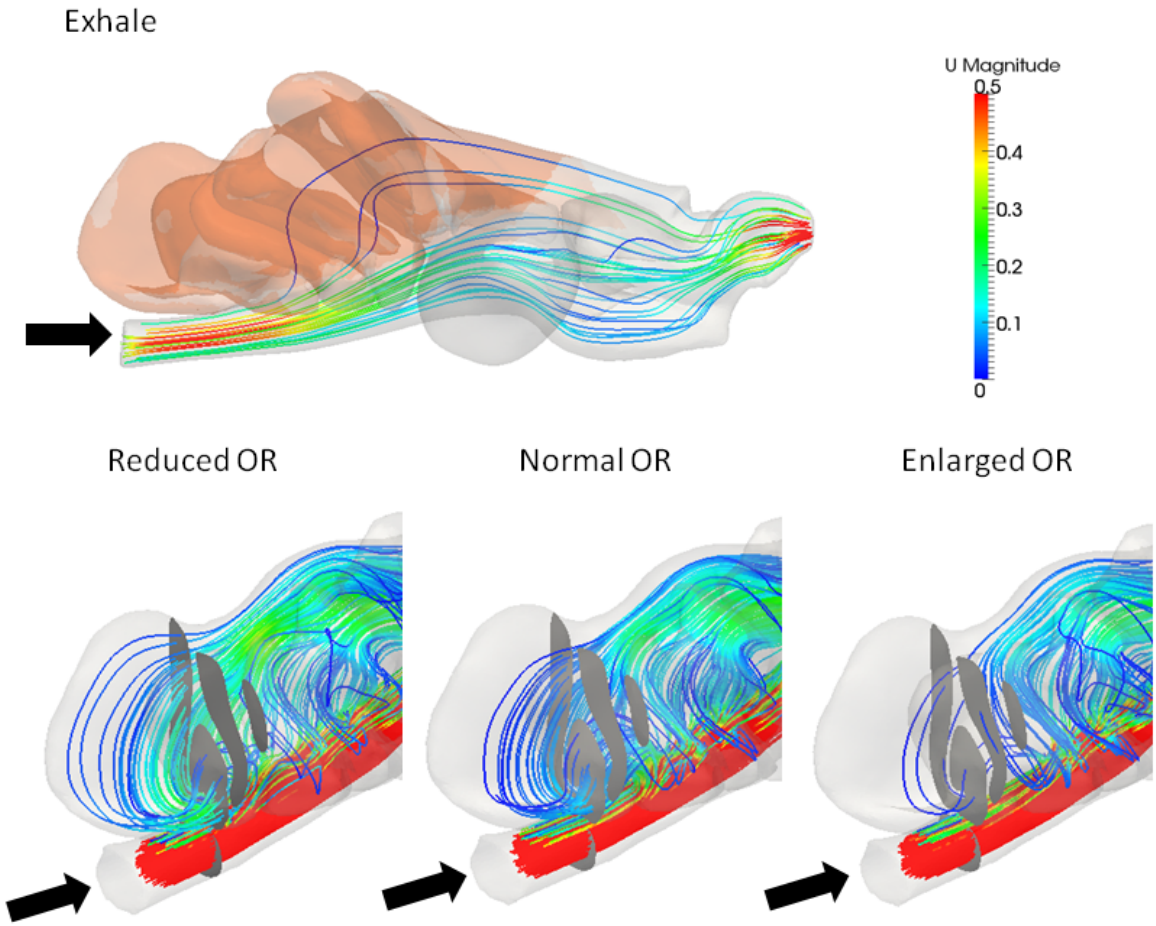

Figure 2.4 Flow patterns during exhalation in *Carollia perspicillata*. The top panel shows a lateral view of the whole airway, with anterior towards the right. Flow is in the direction of the black arrows. The bottom panel shows an oblique latero-posterior view; the grey area is a slice from the same anterior-posterior location across all three models at the beginning of the olfactory recess. "Reduced OR" = model with transverse lamina reduced such that only ~7.5% of the total olfactory epithelium lies within the olfactory recess. "Normal OR" = unmodified model of *Carollia perspicillata*, in which 21.5% of olfactory epithelium lies within the olfactory recess. "Enlarged OR" = model with a lengthened transverse lamina such that ~33% of the total amount of olfactory epithelium lies within the olfactory recess. "U magnitude" refers to the velocity magnitude in m/s. Note that progressively fewer streamlines pass through the slice in models with a longer transverse lamina (i.e. enlarged olfactory recess). Also note how the streamlines that do pass through the olfactory recess are on average slower (more blue in color) in the models with larger olfactory recesses.

CHAPTER 3

PATTERNS AND RATES OF OLFACTORY AIRFLOW IN PHYLLOSTOMID BATS

3.1 Abstract

The morphology of the nasal cavity in mammals with a good sense of smell includes features that are thought to improve olfactory airflow, such as a dorsal conduit that delivers odors quickly to the olfactory mucosa, an enlarged olfactory recess at the back of the airway, and a clear separation of the olfactory and respiratory regions of the nose. The link between these features and having a good sense of smell has been established by detailed functional examinations of only a handful of distantly related mammalian species. In this paper I provide the first detailed examination of olfactory airflow in a group of closely related species that nevertheless differ in their sense of smell. I study six species of phyllostomid bats that have different airway morphologies and foraging ecologies, which have been linked to differences in olfactory ability or reliance. I make qualitative and quantitative comparisons of the patterns and rates of airflow through the olfactory region during both inhalation and exhalation across these six species. Contrary to my expectations, I found no systematic differences among species in either the patterns of airflow through the airway or in rates of flow through the olfactory region. By and large, olfactory airflow seems to be conserved across species. My work suggests that a simple one-to-one mapping of form to function may not exist within the nasal cavity.

3.2 Introduction

Mammals that have a good sense of smell tend to have a suite of morphological features of their nasal cavity that are thought to be adaptations for improved olfactory abilities. These features include a narrow, dorsal conduit through their airway for olfactory airflow, an enlarged cavity (the olfactory recess) at the back of their nasal airway, and a clear separation of the olfactory region of the nose from the respiratory region (Negus, 1958; Moore, 1981; Craven et al., 2007). All of these features impact the way air flows through the nasal cavity. The dorsal conduit delivers inhaled odorant-laden air relatively quickly to the back of the nose, where most of the olfactory epithelium is located (Craven et al., 2010). I refer to this region as the "ethmoturbinate region," because the ethmoturbinate bones, which are lined with olfactory mucosa, occupy this voluminous space. Once air reaches the ethmoturbinate region, it slows down dramatically, and it gradually courses ventrally and laterally, before exiting the airway at the back of the nose along with the respiratory air currents. Part of this ethmoturbinate region is comprised of the olfactory recess, which is a blind pocket at the back of the airway, the principal function of which may be isolating the inhaled, odorant-laden air from exhaled respiratory air currents, which would otherwise "wash out" freshly-inhaled odorants from the ethmoturbinate region (Zhao et al., 2006; Yang et al., 2007a; Craven et al., 2010; Eiting et al., in press).

The link between the morphology of the airway and olfactory airflow is based on detailed functional examinations of only a few species. These studies have tended to focus on extremes in terms of both anatomy and olfactory ability: mammals with a large, restricted olfactory region and a well-developed sense of smell on the one hand (e.g.

dogs, Craven et al. 2007, 2010; rats, Zhao et al., 2006; Yang et al., 2007a,b), and those with a small olfactory region and poorly-developed sense of smell on the other (e.g., humans, (Keyhani et al., 1997; Keyhani et al., 1995). To date, no study has attempted to use a group of closely related species to more precisely link differences in their apparent reliance on olfaction with differences in airway morphology and patterns of airflow. In this paper I attempt to make such a link, which may shed light on the functional and evolutionary relationship between morphological variation and olfactory ability in mammals.

I address this deficiency in my understanding by studying the anatomy and patterns of olfactory airflow in six species of the ecologically-diverse New World Leaf-nosed Bats, which exhibit a broad range of dietary preferences that have been linked to differences in olfactory reliance. My sample includes two basal insectivorous species, *Macrotus waterhousii* and *Mimon crenulatum,* two nectar-feeding bats, *Glossophaga soricina* and *Anoura caudifer*, and two frugivores, *Carollia perspicillata* and *Artibeus jamaicensis* (Fig. 1). Comparative neurobiological studies have consistently demonstrated that fruit- and nectar-feeders have larger olfactory brain structures compared to insectivores of the same brain and body size (Barton et al., 1995; Hutcheon et al., 2002; Safi and Dechmann, 2005). This has led some authors to suggest that diet is a major driving force in the evolution of differently-sized olfactory regions (e.g. Hutcheon et al., 2002). Behavioral studies support this suggestion. In fruit-eating bats like *Artibeus* and *Carollia*, olfactory cues are important in the detection and initial localization of food, and in distinguishing ripe from unripe fruit (Laska, 1990; Altringham and Fenton, 2003). The nectar-feeders *Glossophaga* and *Anoura* also appear to rely on olfactory cues to detect

localized food resources (von Helversen et al., 2000); indeed, the "chiropterophilly" floral syndrome includes characteristic odors (Knudsen and Tollsten, 1995; von Helversen and Voigt, 2002; Pettersson et al., 2004). However, these species generally switch to echolocation as they approach flowers (von Helversen and von Helversen, 2003). Basal insectivores like *Mimon* and *Macrotus* likely do not use olfactory cues when foraging (Altringham and Fenton, 2003). This does not preclude them from using odors in social interactions. For example, the closely related basal insectivore *Phyllostomus discolor* uses odor in mother-pup recognition (Bloss, 1999).

The six species in my study also differ in terms of their nasal airway anatomy (Fig. 1). Fruit-eaters tend to have rostrum that has been anteriorly-posteriorly compressed relative to basal insectivores, which allows them to feed on hard fruits more easily than longer-snouted species (Freeman, 1988; Santana and Dumont, 2009; Dumont et al., 2012). Nectar-feeders, on the other extreme, have an elongated rostrum (to varying degrees), which has had the effect of extending the anterior region of their nasal cavity (Fig. 3.1; Freeman, 2000). This variation in the morphology of the nasal cavity allows me to explicitly test the idea that differences in olfactory reliance during foraging are related to different patterns of olfactory airflow. Specifically, I predict that flow rates through the dorsal conduit will vary, with fruit- and nectar-feeders having higher flow rates compared to insect-feeders, to more rapidly deliver odorants to the ethmoturbinate region. I also predict that fruit- and nectar-feeders will have lower flow rates in the ethmoturbinate region compared to insect-eaters, because lower flow rates improve the efficiency of the olfactory system to absorb odorants (Mozell et al., 1984; Yang et al., 2007b). Finally, I predict that during exhalation, flow will bypass the olfactory recess and ethmoturbinate

region more in fruit- and nectar-feeders compared to insect-feeders, thereby increasing the amount of time odorant molecules are in contact with olfactory receptors lining the ethmoturbinate region.

3.3 Materials and Methods

I constructed three-dimensional models of six species of bats from CT scans generated at the Harvard Center for Nanoscale Systems (Table 3.1). For each species I constructed a 3D Stereolithography (STL) file from the CT scans as follows (see Eiting et al., in press, for additional details). First, an image stack was brought into Mimics v. 16.0 (Materalise, Leuven, Belgium). Once imported, I digitally isolated the airway by using a combination of thresholding and individual editing of slices, with the aid of histological preparations (see Eiting et al., in review, for details of the histological procedure). I converted the airway into an STL file for importing into Geomagic Studio v. 12.0 (3D Systems, Rock Hill, SC, USA), which I used to further refine the details of the model. This refinement was necessary because the fluid dynamics software requires a smooth mesh.

Once the STL file was sufficiently refined, I re-imported the surface model back into Mimics software, which I used to create a solid model of the airway. For each species, this solid model was comprised of approximately 625,000 4-noded tetrahedral elements (Table 3.1). My previous work (Chapter 2) has shown that grid-refinement does not substantially change results, so this number of bricks was judged to be sufficient.

The final, solid model was exported from Mimics as a MSH file, which was compatible with my computational fluid dynamics (CFD) software, OpenFOAM 1.6-ext

(www.openfoam.org). I used OpenFOAM to solve steady-state solutions of inhalation and exhalation (see Appendix B for further information). For each simulation, I applied a constant inflow velocity across the inlet (i.e. the naris during inhalation, and the choana during exhalation), and a zero velocity gradient, constant pressure boundary at the outlet (i.e. the choana during inhalation, and the naris during exhalation). Flow was judged to have reached a steady-state when the velocity residuals fell below 10^{-6}. I scaled the volumetric flow rate in each species by applying the following allometric equation from Craven et al. (2010):

$$Q_{peak} = 1.43M^{1.04+/-0.03}, \quad (1)$$

where Q_{peak} is peak inspiratory flow rate, and M is the body mass (in grams). Each value of Q_{peak} was converted to flow velocity by dividing it by the area of the inlet normal to the direction of flow. The final velocities applied during both inhalation and exhalation for all six models can be seen in Table 1. I performed a sensitivity analysis on flow rate by calculating volumetric flow rate according to the error in the exponent in equation (1); i.e. I calculated a high and low value of Q_{peak} by multiplying M by 1.07 and 1.01. The results were not appreciably different, so I only show the results from using an exponent of 1.04.

To address my hypotheses, I performed both qualitative and quantitative analyses of patterns and rates of flow using the visualization software Paraview v. 4.1.0 (Kitware, Inc., Clifton Park, New York, USA). I compared patterns of flow by studying the location of streamlines (i.e. lines of flow tangential to the direction of flow) for each simulation. I

visualized streamlines by coloring them according to magnitude of the flow velocity. It was necessary to scale the streamline colors to a maximum of 0.3 m/s to achieve a dispersion of colors. In reality, the maximum flow rates (which occurred near the naris and the choana) were roughly an order of magnitude higher than shown in my figures.

In support of my qualitative results, I also compared inhalation flow velocities in the ethmoturbinate region as follows. First, I selected a region in each model that closely approximated the boundary of the ethmoturbinate region. I did this by selecting the first anterior-posterior slice in which I saw a lateral expansion of the nasal airway, and then expanding my selection by including the folded regions interdigitating between ethmoturbinates. I used the pattern of streamlines during inhalation to aid in my selection of parts of the airway to include; areas that were predicted to transmit only respiratory flow were excluded from the selection. Once the ethmoturbinate volume for each species was selected, I calculated the average flow velocity by integrating flow velocity in each brick over the selected volume. For each species, I performed this step a minimum of three times, to assure that my selection procedures and calculations were repeatable. I found variation on the order of 10%, so I report values rounded off to accommodate this uncertainty.

3.4 Results

Patterns of flow during inhalation in all species show that most air passes ventrally through the nasal airway, en route to the nasopharyngeal duct (Fig. 3.2). Air that enters the naris dorsally tends to flow via a dorsal conduit to the rear of the nasal cavity (i.e. the ethmoturbinate region), where most of the olfactory epithelium is located.

Compared to the ethmoturbinate region, flow along the dorsal conduit tends to be faster. Once air from the dorsal conduit reaches the ethmoturbinate region, it slows down substantially. As it does so, it migrates ventrally and laterally (Fig. 3.3), before passing over the transverse lamina and then exiting the airway at the choana, along with the rest of the non-olfactory inhaled air.

I also calculated average flow velocity over the volume of the nasal airway that encompassed the ethmoturbinate region. Calculated flow velocities in this region were in the range of 1.03×10^{-2} m/s to 1.53×10^{-2} m/s (Fig. 3.4a). There are no dramatic differences among the dietary groups, though nectar-feeders do seem to have slightly higher flow rates in the ethmoturbinate region compared to the fruit-eaters. I also standardized flow rates by dividing flow speeds in the ethmoturbinate region by the inhaled flow speed that was applied at the inlet (i.e. naris). Doing so provided me with a velocity-independent metric for how much the air passing through the ethmoturbinate region slows down compared to inhaled flow speeds. Fig. 4b shows that the flow speed in the ethmoturbinate region is on the order of ~1% of the flow speed at the naris; in other words, airflow passes through the olfactory region at only ~1% of the speed with which it enters the nose at the naris. Nectar feeders seem to perform slightly more poorly as judged from this metric, though only by a factor of about four (2.35% in *Anoura geoffroyi* vs. 0.58% in *Artibeus jamaicensis*).

During exhalation in all species, most air again bypasses the ethmoturbinate region on its way through the main airway (Fig. 3.5). However, in all six species my simulations predict that some flow passes through the ethmoturbinate region before exiting at the naris. As during inhalation, exhaled air that passes through the

ethmoturbinate region tends to be much slower than air passing through other parts of the nasal airway.

3.5 Discussion

Despite their morphological and dietary differences, the general patterns and rates of airflow during inhalation are very similar for all six species in my study (Fig. 3.2). They all have a dorsal conduit through which inhaled air flows before reaching the convoluted ethmoturbinate region, where flow speeds decrease substantially. I do not find noticeable variation across species in the rates of flow through this dorsal conduit. From here, air tends to enter the ethmoturbinate region medially (Figs. 3.2, 3.3). Once within the ethmoturbinate complex, air passes laterally and ventrally, before finally meeting up with the respiratory flow and exiting via the choana. The quantitative results confirm these findings. Rates of flow in the ethmoturbinate region do not vary substantially among the six species, ranging only across a factor of 1.5. Even though the flow speed in this region is highest in the nectar-feeding species and lowest in the fruit-eaters, it is not clear whether this variation is meaningful. The flow speeds I see in this region are similar to those seen in rodents (Yang et al., 2007a), suggesting that an optima or range of optima may exist for flow speeds that successfully deliver odorants to olfactory receptors. It is important to point out that flow is primarily delivered by advecting air currents before odorants diffuse out of suspension, meaning that it might be better to analyze flow speeds along specific flow paths (perhaps by analyzing velocity along individual streamlines). Unfortunately, such an analysis is practically infeasible given current modeling technique and computational power.

The patterns of airflow during inhalation seen across all six bat species are very similar to those observed in dogs and rats, suggesting common functional demands for olfactory airflow and performance across a broad array of mammals. During exhalation, however, these bats differ from rodents and dogs, in which exhaled airflow bypasses the olfactory recess en route to leaving via the naris. Rather, in all six species of bats, my models predict that some air passes through the olfactory recess before being finally exhaled. This is especially surprising in species like *Mimon crenulatum* and *Carollia perspicillata*, which have fairly large olfactory recesses with as much as a third of all of their olfactory epithelium located within it (Eiting et al., in review). The implication of this finding is that the primary function of the olfactory recess in these phyllostomid bats may *not* be to sequester recently-inhaled air from expiratory air currents. Instead, the olfactory recess may function to expand the surface area available for olfactory epithelium and slow down inhaled air to improve odorant absorption across the olfactory epithelium. Some computational support for this idea was found by Eiting et al. (in press), who showed in an experimental modeling study that, all else being equal, a larger olfactory recess produces lower rates of flow through this region during exhalation.

The suggestion that the olfactory recess functions to reduce airflow speeds is tentative because the effect that lowering flow speed on odorant transport and deposition may be context-dependent. Studies have fairly consistently shown that higher flow rates produce greater total odorant absorption by the olfactory epithelium; faster flow means more odorant particles are absorbed per unit time (Yang et al., 2007b; Lawson et al., 2012). This could be beneficial to species that are trying to detect environmental odorants in low concentrations. For example, the bat *Carollia perspicillata* is known to increase its

sniffing frequency (and thus its flow rate) when sampling odorants just above threshold concentration, compared to air containing sub-threshold levels of odorants (Laska, 1990). A similar result is also found in the rat (Youngentob et al., 1987). However, higher flow rates also produce less *relative* odorant absorption. In other words, as flow rate increases, a smaller fraction of suspended odorant molecules is absorbed by the olfactory epithelium. This might not be a problem if an animal is trying to detect strong odors, but if a species is for some reason trying to maximize discrimination of odorants, or if odorants are present sporadically or in a finite quantity, improving the absorption efficiency (i.e. relative odorant flux) may be important, and lower flow rates may be expected.

It has long been known that odorants with different solubilities are deposited along different regions of the olfactory mucosa (Moulton, 1976; Mozell, 1966; Yang et al., 2007b; Lawson et al., 2012). This separation of odorants along the path of flow matches to a first approximation the location of the relevant olfactory receptors that are expressed within the olfactory epithelium (Ressler et al., 1993; Schoenfeld and Cleland, 2006). Performing transient analyses of odorant deposition would be an informative way to examine the generality of the hypothesized link between the "inherent" pattern of olfactory gene expression and the "imposed" pattern of odorant delivery by inhaled air (terminology after Moulton, 1976). Such analyses would also allow me to generate hypotheses about the location and relative abundance of particular types of olfactory gene receptors expressed throughout the epithelium, and the possible link with ecologically-relevant odors.

My results also add to the growing body of work that shows functional similarity can occur despite morphological variability (so called many-to-one mapping, Alfaro et al., 2004; Wainwright et al., 2005). In the four bar linkage system of fish jaws, for instance, functional equivalence (in terms of kinematic transmission) can be produced from a variety of morphologically-distinct phenotypes (Hulsey and Wainwright, 2002). The consequences for this many-to-one mapping of form onto function include a reduced ability to infer function from morphology and the possibility for lineages to explore alternate routes to diversity—both morphological and functional (Wainwright et al., 2005). Despite the extensive variation in the shapes of the nasal passages in phyllostomid bats, the patterns and rates of airflow across the clade appear very similar (Figs. 3.2-3.5). These results suggest that olfactory airflow and its relationship to the morphology of the nasal airways may be another case of many-to-one mapping in the vertebrate cranium. If true, the morphology of the airway may not be under strong selection pressure to change with shifting functional demands. It could also be the case that the relatively invariant patterns and rates of flow that I see are the result of phylogenetic effects. In this scenario, ancestral phyllostomids may have had a morphology already well-suited for olfaction, perhaps because of the emphasis that bats (and mammals in general) place on olfaction to mediate communication (Anisko, 1976). Using olfaction to aid in foraging for may have been a relatively easy addition to species that already rely on olfaction for other functions. A third explanation for the patterns I see may be that the nose and nasal cavity are developmentally constrained by the numerous structures of the cranium, such as the brain, dentition, and eyes. The nasal cavity of phyllosomid bats also transmits echolocation calls, which may act as an additional agent of selection on the morphology

of the nasal cavity (Pedersen, 1993; Pedersen, 1995). Disentangling these various explanations would be an exciting avenue for future research.

3.6 Conclusions

Despite extensive morphological differences in the nasal cavity of six phyllostomid bats, I do not find substantial functional differences in the patterns and rates of olfactory airflow during inhalation or exhalation. Dietary differences between these species suggested that variation in olfactory airflow may have been expected, so my finding in light of this expectation was suprising. Instead, my work suggests that morphology is decoupled from olfactory function in the nasal cavity, thereby hinting at alternative explanations for the morphological variation seen in these species. Such factors could include relaxed selection, phylogenetic relationships, or developmental constraints. Investigating these and other factors would be a valuable addition to our understanding of the mammalian nasal cavity.

Table 3.1 Details of the specimens and scanning & model parameters used in this study.

Species	AMNH #	Pixel size (µm)	# Bricks in Final Model	Average Body Mass (g)	Diet[f]
Macrotus waterhousii	275472	19.9	622448	16[a]	I
Mimon crenulatum	267888	18.2	636550	14.5[b]	I
Anoura geoffroyi	199538	24.3	616119	12.8[c]	N
Glossophaga soricina	260965	19	622685	10[d]	N
Carollia perspicillata	261433	24.3	623269	18.5[e]	F
Artibeus jamaicensis	267998	26.7	633591	48[b]	F

[a]Hosken, 1997

[b]Santana and Dumont, 2009

[c]Ortega and Alarcón-D., 2008

[d]Alvarez et al., 1991

[e]Cloutier and Thomas, 1992

[f]Ferrarezi and Gimenez, 1996

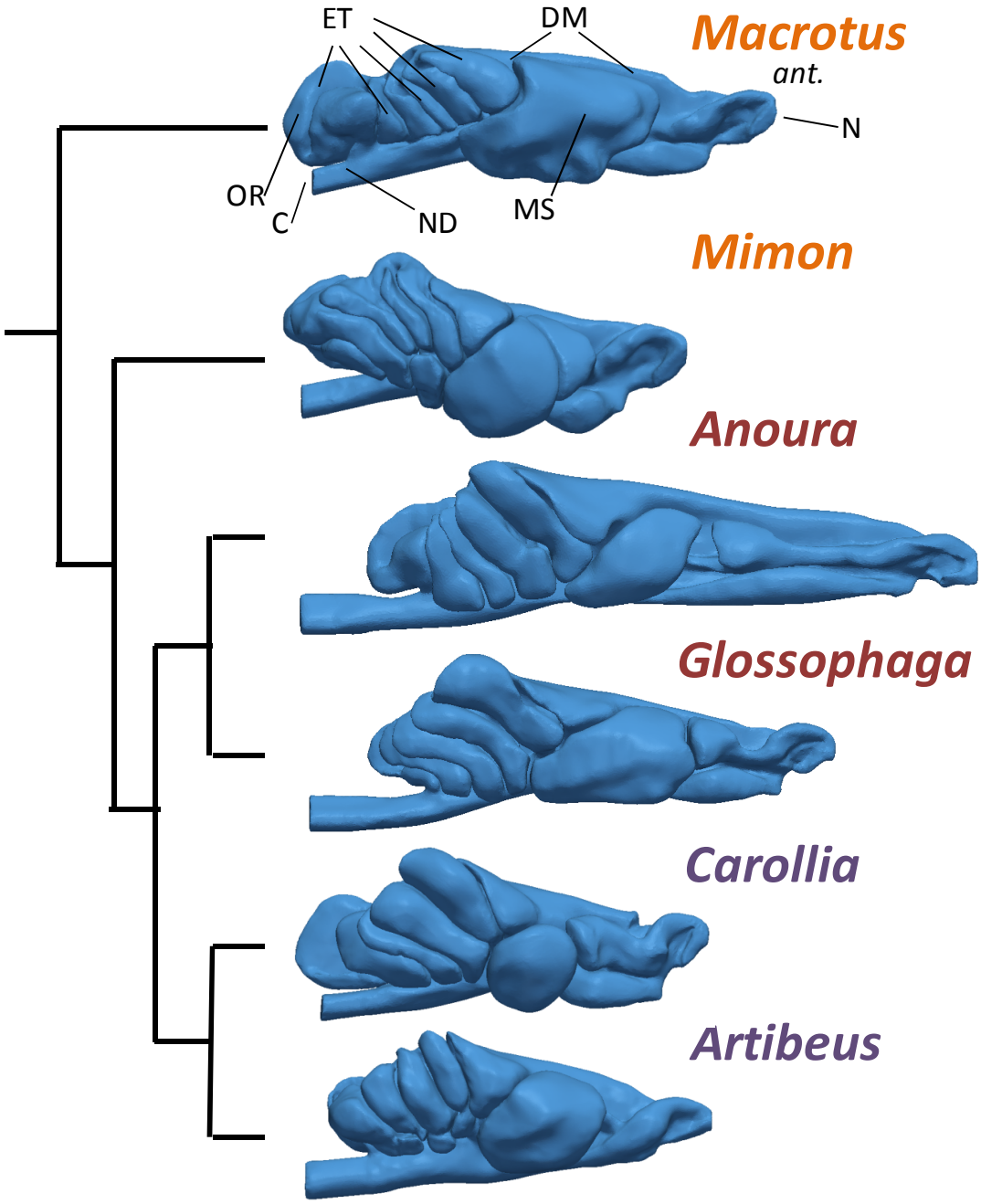

Figure 3.1 Phylogenetic relationships of the six species of bats used in my study, together with a lateral view of the right nasal airway for each species. 3D models are scaled to the same height, to give a sense of the dimensions of the airway regardless of size. Names of taxa are color-coded to reflect diet: orange = insects, maroon = nectar, lavender = fruit. ant. = anterior, C = choana, DM = dorsal meatus, ET = ethmoturbinate region, MS = maxillary sinus, N = naris, ND = nasopharyngeal duct, OR = olfactory recess.

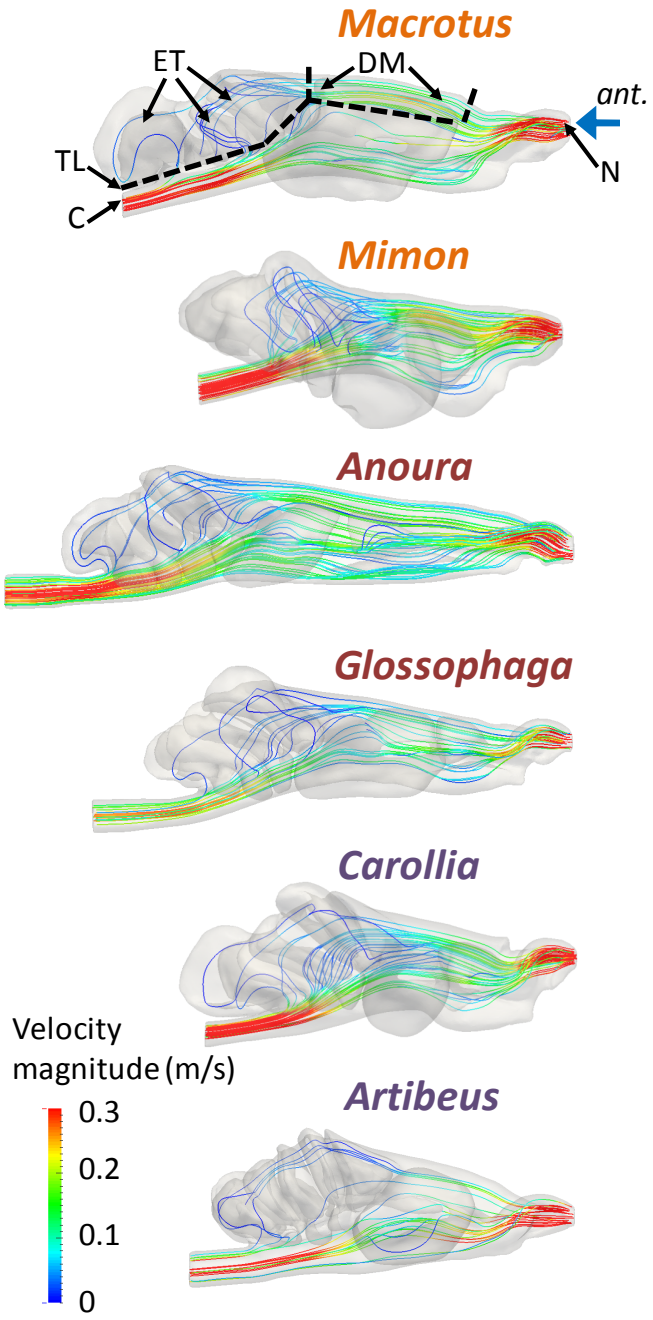

Figure 3.2 Lateral view of right nasal cavity showing patterns and rates of airflow during inhalation. Flow paths are shown as streamlines, and rates of flow are shown in color. Inhaled air was forced through the naris (N) in the direction of the large blue arrow. Streamlines are scaled to the same velocity magnitude in all six models. Note in general how a dorsal meatus (DM) of relatively high flow speeds delivers air to the more posterior ethmoturbinate region (ET), where flow speeds tend to be lower. After passing through the ethmoturbinate region, flow passes over the transverse lamina (TL) and exits at the choana (C). ant. = anterior.

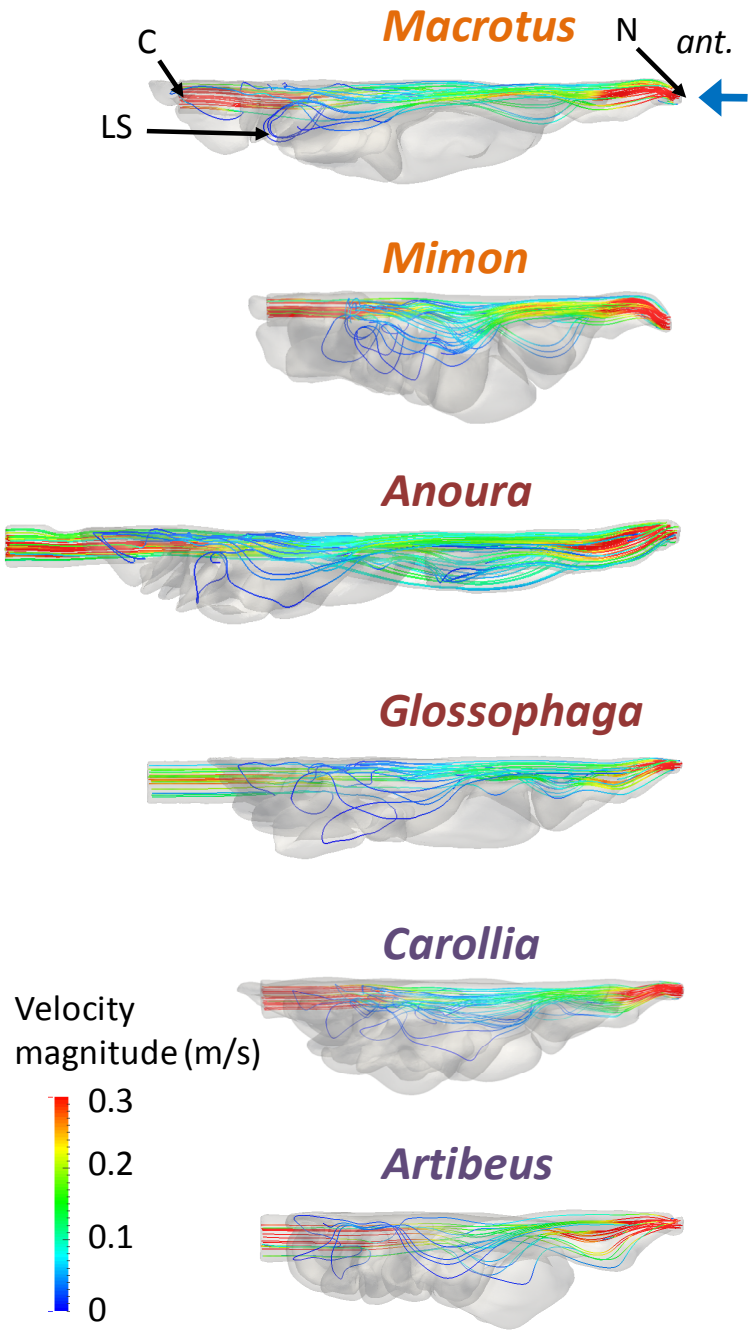

Figure 3.3 Dorsal view of right nasal cavity showing patterns and rates of airflow during inhalation. Flow paths are shown as streamlines, and rates of flow are shown in color. Inhaled air was forced through the naris (N) in the direction of the large blue arrow. Streamlines are scaled to the same velocity magnitude in all six models. Note the lateral streamlines (LS) that migrate ventrally and laterally before exiting at the choana (C). c.f. Figure 3.2. ant. = anterior.

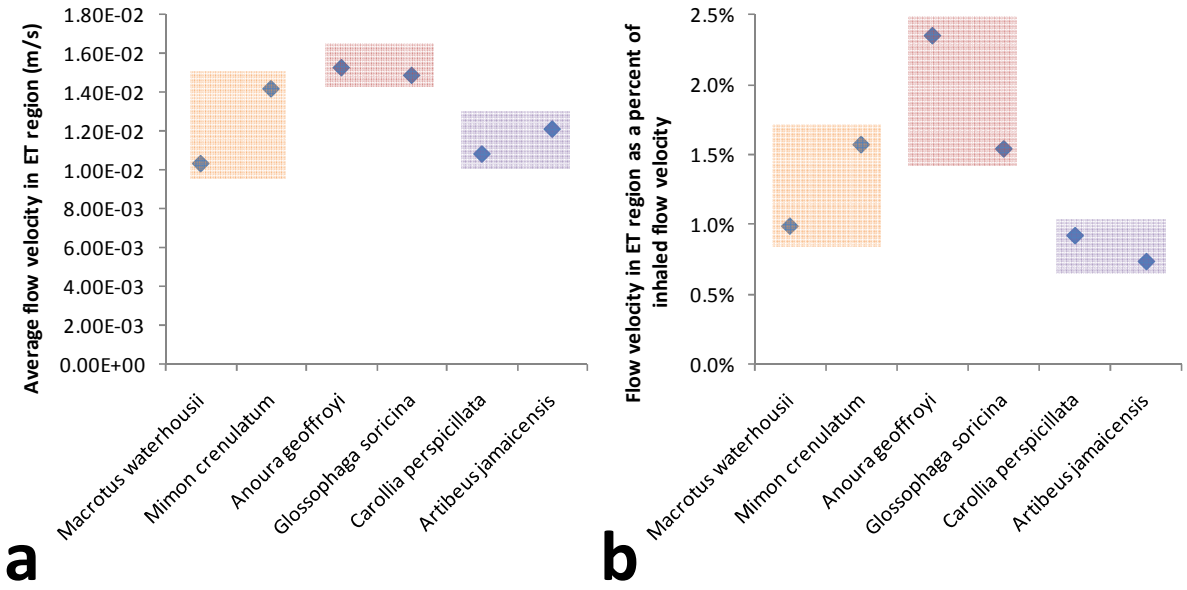

Figure 3.4 Flow velocities during inhalation. (a) Average flow velocity in the ethmoturbinate region across six species of bats. (b) Relative flow velocity in the ethmoturbinate region (i.e. ethmoturbinate velocity divided by velocity at the inlet) across six species of bats, expressed as a percentage. In both plots, species are enclosed within a box that is color-coded according to diet as in Figure 3.1.

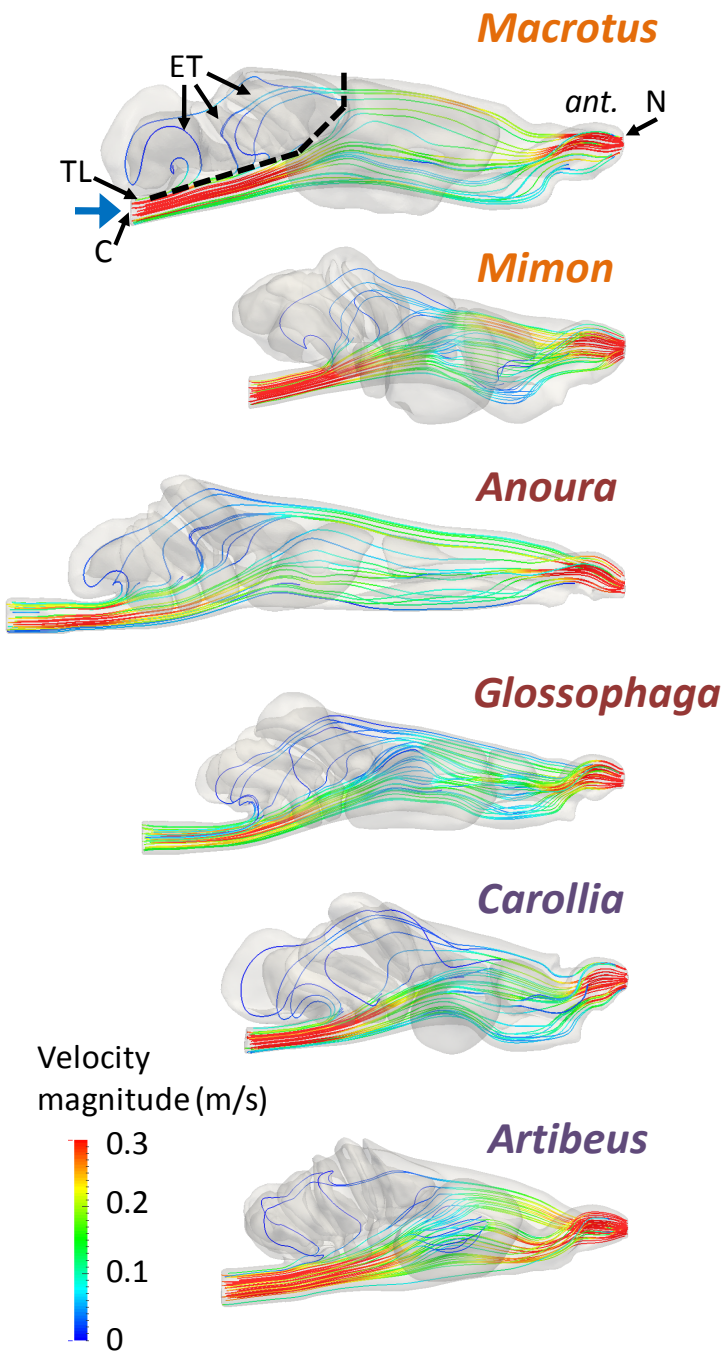

Figure 3.5 Lateral view of the right nasal cavity showing patterns and rates of airflow during exhalation. The paths of flow are indicated by streamlines, and rates of flow are indicated by color. Exhaled air was forced through the nasopharyngeal duct at the location of the large blue arrows. Streamlines are scaled to the same velocity magnitude in all six models. Note in general how streamlines pass through the olfactory/ethmoturbinate region (ET), suggesting that this region is not isolated from expiratory airflow. Labels as in Figure 3.2.

APPENDIX A

PRIMARY DATA FOR 12 SPECIES OF BATS USED IN CHAPTER 1

OSNs = number of olfactory sensory neurons, # MCs = number of mitral cells, OB volume = volume of olfactory bulb,
Diet categories: F = fruit-eater, I = insect-eater, N = nectar-feeder

Species	n	# OSNs	# MCs	# Glomeruli	Specimen Numbers	n	OB Volume (mm^3)[a]	Brain Volume (mm^3)[a]	Diet[b]
Anoura geoffroyi	2	3.2E+06	1.3E+04	318	MNH 199538, KPB 95P002[d]	3	9.1	279.2	N
Artibeus cinereus	1	6.2E+06	1.0E+04	632	AMNH 265585	3	9.45	221.75	F
Artibeus jamaicensis	2	1.4E+07	1.4E+04	697	AMNH 267998, 268528	3	19.35	481.25	F
Carollia perspicillata	2	7.2E+06	1.7E+04	533	AMNH 261433, 261453	3	13.15	258.5	F
Glossophaga soricina	2	2.8E+06	1.0E+04	312	AMNH 260958, 260965	3	5.75	187.4	N
Lophostoma silvicola	1	2.9E+06	9.1E+03	268	AMNH 267422	1	7.3	356.7	I
Micronycteris microtis[c]	1	3.5E+06	8.1E+03	308	AMNH 143773	3	5.15	129.4	I
Mimon crenulatum	1	2.1E+06	1.2E+04	346	AMNH 267888	2	3.65	153.65	I
Phyllostomus hastatus	1	1.2E+07	1.5E+04	590	AMNH 48360	3	21.4	719.25	I
Sturnira lilium	2	6.5E+06	1.1E+04	622	AMNH 189885, 189946	3	14.2	292	F
Trachops cirrhosus	1	5.1E+06	9.8E+03	303	AMNH 235555	2	11.75	474.6	I
Uroderma bilobatum	2	6.6E+06	1.3E+04	594	AMNH 260209, UM 3034	3	14.35	290.05	F

a: Data from Baron et al. (1996)

b: Data from Ferrerezi and Gimenez (1996)

c: OB vol. and Brain vol. from *Micronycteris megalotis* ; *M. microtis* was formerly a subspecies of *M. megalotis;* AMNH specimens were originally *M. megalotis microtis* ; data from Baron et al. (1996) do not provide subspecies

d: specimen from the collection of Kunwar P Bhatnagar and curated by TDS; see Bhatnagar and Smith (2007) for details on histological procedures

APPENDIX B

ADDITIONAL DETAILS ON CREATING AND USING BIOMECHANICAL MODELS FROM CHAPTERS 2 AND 3

B.1. Running Analyses in OpenFOAM

I performed all analyses in OpenFOAM v. 1.6-ext (www.openfoam.org), running on the parallel cluster "Cyclops," which is housed in the College of Engineering at the University of Massachusetts. In the OpenFOAM system, analyses are run as a series of "cases," where each case has its own subdirectory. I performed analyses as follows. First, solid models of the airspace of the right nasal cavity, consisting of approximately 625,000 4-noded tetrahedral elements (depending on the species; see Table 3.1), were exported as Fluent MSH files from the modeling software Mimics. I then imported the models to my personal user directory on Cyclops (specifically, to my "run" subdirectory), where I converted them from Fluent mesh format to OpenFOAM format (using the command "FluentMeshToFoam," sometimes including the addendum, " -scale 0.001," to convert the mesh from millimeters to meters, as needed). Once converted, I ran the utility "checkMesh" to ensure the sizes of elements was correct, to identify severely non-orthogonal elements, and to check that the maximum skewness was below ~8-10.I set up the rest of the "case" folder by seeding it with subfolders devoted to calculations used in the CFD solutions ("system"), to specifying the mesh and physical properties of the system ("constant"), and to the temporal nature of the calculation, which represents the initial conditions ("0").

All of my cases were solved by using the "icoFoam" solver, so this determined which files to include in my analyses, and the content of those files. I set kinematic viscosity to 1.6×10^{-5} m^2/s. Please consult the user guide on www.openfoam.org for additional details on the content of the files within each of the subdirectories. Each model had three boundary fields, which were "inlet," "outlet," and "wall." I applied different boundary conditions (in the "0" directory) to each of these three fields. In my simulations forced air through the inlet by specifying velocity at the naris during inhalation or at the choana during exhalation. Thus, my velocity file had a fixed uniform value at the inlet and at the wall (which was always uniform zero to indicate no air moving through the wall.) The outlet was always set to zero gradient. For the pressure file, both the inlet and the wall were set to zero gradient, while the outlet was set to uniform zero. An example velocity file looks as follows (using the values for inhalation in *Artibeus jamaicensis*; pressure files look very similar):

```
/*--------------------------------*- C++ -*----------------------------------*\
| =========                 |                                                 |
| \\      /  F ield         | OpenFOAM: The Open Source CFD Toolbox           |
|  \\    /   O peration     | Version:  1.6-ext                               |
|   \\  /    A nd           | Revision: 1745                                  |
|    \\/     M anipulation  | Web:      http://www.OpenFOAM.org               |
\*---------------------------------------------------------------------------*/
FoamFile
{
    version     2.0;
    format      ascii;
    class       volVectorField;
    location    "0";
    object      U;
}
// * * * * * * * * * * * * * * * * * * * * * * * * * * * * * * * * * * * * * //

dimensions      [0 1 -1 0 0 0 0];

internalField   uniform (1.64 0 0);

boundaryField
{
    wall
    {
        type            fixedValue;
        value           uniform (0 0 0);
    }
    inlet
    {
        type            fixedValue;
        value           uniform (1.64 0 0);
    }
    outlet
    {
        type            zeroGradient;
    }
}


// ************************************************************************* //
```

All of the simulations I performed were of steady-state airflow. In order for the solution to reach steady-state, I allowed each simulation to run until the maximum velocity of the system did not change appreciably after many time steps (usually several hundred), and the initial velocity residuals were on the order of 1×10^{-4}. Convergence judged in this manner was usually achieved in the range of 2000 – 10,000 time steps. Minimum time step was set so that the CFL number was much less than 1, and usually resulted in a time step of 1×10^{-6} s. Here is a sample of the "controlDict" file from the

inhale case for *Artibeus jamaicensis*, showing time control and several other parameters necessary to run a successful case:

```
FoamFile
{
    version     2.0;
    format      ascii;
    class       dictionary;
    object      controlDict;
}

application icoFoam;

startFrom       latestTime;

startTime       0;

stopAt          endTime;

endTime         0.02;

deltaT          0.000001;

writeControl    timeStep;

writeInterval   1000;

purgeWrite      0;

writeFormat     ascii;

writePrecision  6;

writeCompression uncompressed;

timeFormat      general;

timePrecision   6;

runTimeModifiable yes;
```

Once all of the files in the subdirectories were ready, I split all of the folders and files into 32 components to prepare for parallel processing. I used the method “scotch” to break-up the files, which was carried out by running the command “decomposePar” from Cyclops. I included one additional file, “runfile,” in the directory for each particular case. In this file I included all of the information necessary to run the solver using the Portable Batch System. This file includes necessary commands for how many processors

to use, how much clock time is needed, where to save the output, and what processor to use. Here is an example runfile, again using the case of *Artibeus jamaicensis* inhalation:

```
#!/bin/bash
### PBS script for CYCLOPS - GENERIC
### MBM 7.1.09
#####################################################
### Queue name
#PBS -q standard
### Job name
#PBS -N artibeus-inhale01
### Output and Error file names ... uncomment if not
### using execname > outputfile & option
###PBS -e error.info
###PBS -o code.info
### Join output and error files
#PBS -j oe
### Specify the number of nodes (nodes) and
### the number of processors / cores to use
### per node (ppn)
#PBS -l nodes=8:ppn=4:top64
### where region=long or top64 (see doc)
### Specify how much wall clock time is needed
#PBS -l walltime=24:00:00
#####################################################
### This job's working directory
echo Working directory is $PBS_O_WORKDIR
cd $PBS_O_WORKDIR
echo Running on host `hostname`
echo Time is `date`
echo Directory is `pwd`
echo This jobs runs on the following processors:
echo `cat $PBS_NODEFILE`

### Define number of processors
NPROCS=`wc -l < $PBS_NODEFILE`
echo This job has allocated $NPROCS cores

### Run the parallel MPI executable
mpiexec-pbs icoFoam -parallel > logfile-artibeus-inh01
```

After the simulation reached convergence, I stitched back together the 32 separate subfolders for each processer using the command, “reconstructPar.” Then, I converted the solution to VTK format with the command, “foamToVTK.” Once completed, I copied all files to a local directory for post-processing and visualization using Paraview. Paraview is a user-friendly program for which many tutorials and helpful instructional materials have been written, so I will not go into further detail on it here.

B.2. Grid Refinement

To assess sensitivity of the simulation results to the size of grid elements, I performed a very basic grid refinement study on the inhalation condition of the model of *Carollia perspicillata*. After generating a solid mesh in Mimics, I doubled and quadrupled the number of tetrahedral elements by reducing the maximum length of a tetrahedral, thereby forcing there to be more bricks populating the model. After generating 2X and 4X refined models, I performed all of the same steps for running a model as in the case for the unrefined model (see section B.1). During post-processing I calculated maximum and average velocities for my domain, and I also examined streamlines scaled to the same velocity magnitude, to assess for differences in the patterns of airflow. The results from this study indicated the refining the grid beyond my initial ~625,000 number of bricks did not have a noticeable effect. Velocity values did not differ between the models, and neither did the patterns of airflow. These results led me to just consider the ~625,000-brick models for all subsequent analyses.

BIBLIOGRAPHY

Alfaro, M. E., Bolnick, D. I. and Wainwright, P. C. (2004). Evolutionary dynamics of complex biomechanical systems: an example using the four-bar mechanism. *Evolution* **58,** 495-503.

Allison, A. and Warwick, R. T. (1949). Quantitative observations on the olfactory system of the rabbit. *Brain* **72,** 186-197.

Altringham, J. and Fenton, M. (2003). Sensory ecology and communication in the Chiroptera. In *Bat Ecology* (ed. T. Kunz and M. Fenton), pp. 90-127. Chicago: University of Chicago Press.

Alvarez, J., Willig, M. R., Jones Jr., J. K., Webster, W. D. (1991). *Glossophaga soricina*. *Mamm. Species* **379,** 1-7.

Anisko, J. J. (1976). Communication by chemical signals in Canidae. In *Mammalian olfaction, reproductive processes and behavior* (ed. R. L. Doty), pp. 283-293. New York: Academic Press.

Baron, G., Frahm, H., Bhatnagar, K. and Stephan, H. (1983). Comparison of brain structure volumes in Insectivora and Primates. III. Main olfactory bulb (MOB). *J. Hirnforsch.* **24,** 551-568.

Baron, G., Stephan, H. and Frahm, H. D. (1996). *Comparative neurobiology in Chiroptera*. Basel: Birkhäuser.

Barton, R. A. (2006). Olfactory evolution and behavioral ecology in primates. *Am. J. Primatol.* **68,** 545-558.

Barton, R. A., Purvis, A. and Harvey, P. H. (1995). Evolutionary radiation of visual and olfactory brain systems in primates, bats and insectivores. *Philos. Trans. R. Soc. Lond. B. Biol. Sci.* **348,** 381-392.

Bhatnagar, K. P. and Kallen, F. C. (1974). Cribriform plate of ethmoid, olfactory bulb and olfactory acuity in forty species of bats. *J. Morphol.* **142,** 71-89.

Bhatnagar, K. P. and Smith, T. D. (2007). Light microscopic and ultrastructural observations on the vomeronasal organ of *Anoura* (Chiroptera: Phyllostomidae). *Anat. Rec.* **290,** 1341-1354.

Bloss, J. (1999). Olfaction and the use of chemical signals in bats. *Acta Chiropterol.* **1,** 31-45.

Cleland, T. A. and Linster, C. (2005). Computation in the olfactory system. *Chem. Senses* **30,** 801-813.

Cloutier, D. and Thomas, D. W. (1992). *Carollia perspicillata*. *Mamm. Species* **417,** 1-9.

Craven, B. A., Neuberger, T., Paterson, E. G., Webb, A. G., Josephson, E. M., Morrison, E. E. and Settles, G. S. (2007). Reconstruction and morphometric analysis of the nasal airway of the dog (Canis familiaris) and implications regarding olfactory airflow. *Anat. Rec.* **290,** 1325-1340.

Craven, B. A., Paterson, E. G. and Settles, G. S. (2010). The fluid dynamics of canine olfaction: unique nasal airflow patterns as an explanation of macrosmia. *Journal of The Royal Society Interface* **7,** 933-943.

Dumont, E. R., Dávalos, L. M., Goldberg, A., Santana, S. E., Rex, K. and Voigt, C. C. (2012). Morphological innovation, diversification and invasion of a new adaptive zone. *Proc. Roy. Soc. B* **279,** 1797-1805.

Eiting, T., Perot, J., Smith, T. and Dumont, E. (in press). The role of the olfactory recess in olfactory airflow. *J Exp Biol*.

Eiting, T., Smith, T. and Dumont, E. (in review). Olfactory epithelium in the olfactory recess: a case study in New World Leaf-nosed Bats. *Anat. Rec.*

Farbman, A. I. (1992). *Cell biology of olfaction*, pp. 282. New York, NY: Cambridge University Press.

Ferrarezzi, H. and Gimenez, E. (1996). Systematic patterns and the evolution of feeding habits in Chiroptera (Archonta: Mammalia). *J. Comp. Biol.* **1,** 75-94.

Firestein, S. (2001). How the olfactory system makes sense of scents. *Nature* **413,** 211-218.

Freeman, P. W. (2000). Macroevolution in Microchiroptera: Recoupling morphology and ecology with phylogeny. *Evol. Ecol. Res.* **2,** 317-335.

Freeman, P. W. (1988). Frugivorous and animalivorous bats (Microchiroptera): dental and cranial adaptations. *Biol. J. Linn. Soc.* **33,** 249-272.

Gittleman, J. L. (1991). Carnivore olfactory bulb size: allometry, phylogeny and ecology. *J. Zool.* **225,** 253-272.

Gundersen, H. and Jensen, E. (1987). The efficiency of systematic sampling in stereology and its prediction. *J. Microsc.* **147,** 229-263.

Gundersen, H., Jensen, E., Kieu, K. and Nielsen, J. (1999). The efficiency of systematic sampling in stereology—reconsidered. *J. Microsc.* **193,** 199-211.

Harmon, L. J., Weir, J. T., Brock, C. D., Glor, R. E. and Challenger, W. (2008). GEIGER: investigating evolutionary radiations. *Bioinformatics* **24,** 129-131.

Hayden, S., Bekaert, M., Crider, T. A., Mariani, S., Murphy, W. J. and Teeling, E. C. (2010). Ecological adaptation determines functional mammalian olfactory subgenomes. *Genome Res.* **20,** 1-9.

Healy, S. and Guilford, T. (1990). Olfactory-bulb size and nocturnality in birds. *Evolution* **44,** 339-346.

Hepper, P. G. and Wells, D. L. (2012). Olfactory discrimination in the western lowland gorilla, Gorilla gorilla gorilla. *Primates* **53,** 121-126.

Herculano-Houzel, S., Mota, B. and Lent, R. (2006). Cellular scaling rules for rodent brains. *Proc. Natl. Acad. Sci. USA* **103,** 12138-12143.

Herculano-Houzel, S., Collins, C. E., Wong, P. and Kaas, J. H. (2007). Cellular scaling rules for primate brains. *Proc. Natl. Acad. Sci. U. S. A.* **104,** 3562-3567.

Hosken, D. (1997). Sperm competition in bats. *Proc. Roy Soc. B* **264,** 385-392.

Hulsey, C. D. and Wainwright, P. C. (2002). Projecting mechanics into morphospace: disparity in the feeding system of labrid fishes. *Proc. Biol. Sci.* **269,** 317-326.

Hutcheon, J. M., Kirsch, J. A. W. and Garland Jr., T. (2002). A comparative analysis of brain size in relation to foraging ecology and phylogeny in the Chiroptera. *Brain, Behav. and Evol.* **60,** 165-180.

Joshi, D., Völkl, M., Shepherd, G. M. and Laska, M. (2006). Olfactory sensitivity for enantiomers and their racemic mixtures—A comparative study in CD-1 mice and spider monkeys. *Chem. Senses* **31,** 655-664.

Keyhani, K., Scherer, P. W. and Mozell, M. M. (1997). A numerical model of nasal odorant transport for the analysis of human olfaction. *J. Theor. Biol.* **186,** 279-301.

Keyhani, K., Mozell, M. and Scherer, P. (1995). Numerical simulation of airflow in the human nasal cavity. *J. Biomech. Eng.* **117,** 429-441.

Knudsen, J. T. and Tollsten, L. (1995). Floral scent in bat-pollinated plants: a case of convergent evolution. *Bot. J. Linn. Soc.* **119,** 45-57.

Korine, C. and Kalko, E. K. V. (2005). Fruit detection and discrimination by small fruit-eating bats (Phyllostomidae): echolocation call design and olfaction. *Behav. Ecol. Sociobiol.* **59,** 12-23.

Laska, M. (1990). Olfactory discrimination ability in short-tailed fruit bat, Carollia perspicillata (Chiroptera: Phyllostomatidae). *J. Chem. Ecol.* **16,** 3291-3299.

Laska, M., Genzel, D. and Wieser, A. (2005). The number of functional olfactory receptor genes and the relative size of olfactory brain structures are poor predictors of olfactory discrimination performance with enantiomers. *Chem. Senses* **30,** 171-175.

Laska, M., Seibt, A. and Weber, A. (2000). 'Microsmatic' primates revisited: olfactory sensitivity in the squirrel monkey. *Chem. Senses* **25,** 47-53.

Laska, M. and Shepherd, G. M. (2007). Olfactory discrimination ability of CD-1 mice for a large array of enantiomers. *Neuroscience* **144,** 295-301.

Lawson, M., Craven, B., Paterson, E. and Settles, G. (2012). A Computational Study of Odorant Transport and Deposition in the Canine Nasal Cavity: Implications for Olfaction. *Chem. Senses* **37,** 553-566.

Lent, R., Azevedo, F. A., Andrade-Moraes, C. H. and Pinto, A. V. (2012). How many neurons do you have? Some dogmas of quantitative neuroscience under revision. *Eur. J. Neurosci.* **35,** 1-9.

Mombaerts, P., Wang, F., Dulac, C., Chao, S. K., Nemes, A., Mendelsohn, M., Edmondson, J. and Axel, R. (1996). Visualizing an olfactory sensory map. *Cell* **87,** 675-686.

Moore, W. J. (1981). *The Mammalian Skull*, pp. 369. Cambridge, UK: Cambridge University Press.

Moulton, D. G. (1976). Spatial patterning of response to odors in the peripheral olfactory system. *Physiol. Rev.* **56,** 578-593.

Mouton, P. R. (2011). *Unbiased stereology: A concise guide*. Baltimore: The Johns Hopkins University Press.

Mozell, M. M., Sheehe, P. R., Swieck, S., Kurtz, D. B. and Hornung, D. E. (1984). A parametric study of the stimulation variables affecting the magnitude of the olfactory nerve response. *J. Gen. Physiol.* **83,** 233-267.

Mozell, M. M. (1966). The spatiotemporal analysis of odorants at the level of the olfactory receptor sheet. *J. Gen. Physiol.* **50,** 25-41.

Negus, V. (1958). *The comparative anatomy and physiology of the nose and paranasal sinuses*, pp. 379. Edinburgh: Livingstone.

Ortega, J. and Alarcón-D., I. (2008). *Anoura geoffroyi* (Chiroptera: Phyllostomidae). *Mamm. Species* **818**, 1-7.

Pagel, M. (1999). Inferring the historical patterns of biological evolution. *Nature* **401,** 877-884.

Paradis, E., Claude, J. and Strimmer, K. (2004). APE: analyses of phylogenetics and evolution in R language. *Bioinformatics* **20,** 289-290.

Pedersen, S. C. (1993). Cephalometric correlates of echolocation in the Chiroptera. *J. Morphol.* **218,** 85-98.

Pedersen, S. C. (1995). Cephalometric correlates of echolocation in the Chiroptera: II. Fetal development. *J. Morphol.* **225,** 107-123.

Pettersson, S., Ervik, F. and Knudsen, J. T. (2004). Floral scent of bat-pollinated species: West Africa vs. the New World. *Biol. J. Linn. Soc.* **82,** 161-168.

Pihlström, H. (2008). Comparative anatomy and physiology of chemical senses in aquatic mammals. In *Sensory evolution on the threshold: adaptations in secondarily aquatic vertebrates* (ed. J. Thewissen and S. Nummela), pp. 95-109. Berkeley, CA: University of California Press.

Price, J. and Powell, T. (1970). The mitral and short axon cells of the olfactory bulb. *J. Cell. Sci.* **7,** 631-651.

R Core Team. (2012). *R: A language and environment for statistical computing.* Vienna: R Foundation for Statistical Computing. Available at http://www.R-project.org/.

Ressler, K. J., Sullivan, S. L. and Buck, L. B. (1993). A zonal organization of odorant receptor gene expression in the olfactory epithelium. *Cell* **73,** 597-609.

Revell, L. J. (2010). Phylogenetic signal and linear regression on species data. *Methods Ecol. Evol.* **1,** 319-329.

Rizvanovic, A., Amundin, M. and Laska, M. (2013). Olfactory discrimination ability of Asian elephants (Elephas maximus) for structurally related odorants. *Chem. Senses* **38,** 107-118.

Royet, J., Distel, H., Hudson, R. and Gervais, R. (1998). A re-estimation of the number of glomeruli and mitral cells in the olfactory bulb of rabbit. *Brain Res.* **788,** 35-42.

Safi, K. and Dechmann, D. K. N. (2005). Adaptation of brain regions to habitat complexity: a comparative analysis in bats (Chiroptera). *Proc. Roy. Soc. B* **272,** 179-186.

Santana, S. and Dumont, E. (2009). Connecting behaviour and performance: the evolution of biting behaviour and bite performance in bats. *J. Evol. Biol.* **22,** 2131-2145.

Sarko, D. K., Catania, K. C., Leitch, D. B., Kaas, J. H. and Herculano-Houzel, S. (2009). Cellular scaling rules of insectivore brains. *Front. Neuroanat.* **3,** 8.

Schoenfeld, T. A. and Cleland, T. A. (2006). Anatomical Contributions to Odorant Sampling and Representation in Rodents: Zoning in on Sniffing Behavior. *Chem. Senses* **31,** 131-144.

Schoenfeld, T. A. and Knott, T. K. (2004). Evidence for the disproportionate mapping of olfactory airspace onto the main olfactory bulb of the hamster. *The Journal of Comparative Neurology* **476,** 186-201.

Shepherd, G. M. (2003). *The synaptic organization of the brain*. New York: Oxford University Press.

Smith, T. D. and Bhatnagar, K. P. (2004). Microsmatic primates: reconsidering how and when size matters. *Anat. Rec.* **279,** 24-31.

Thies, W., Kalko, E. K. V. and Schnitzler, H. U. (1998). The roles of echolocation and olfaction in two Neotropical fruit-eating bats, *Carollia perspicillata* and *C. castanea*, feeding on *Piper*. *Behav. Ecol. Sociobiol.* **42,** 397-409.

Von Helversen, D. and Von Helversen, O. (2003). Object recognition by echolocation: a nectar-feeding bat exploiting the flowers of a rain forest vine. *Journal of Comparative Physiology A* **189,** 327-336.

von Helversen, O., Winkler, L. and Bestmann, H. (2000). Sulphur-containing "perfumes" attract flower-visiting bats. *J. Comp. Physiol. A* **186,** 143-153.

von Helversen, O. and Voigt, C. C. (2002). Glossophagine bat pollination in Helicteres baruensis (Sterculiaceae). *Ecotropica* **8,** 23-30.

Wainwright, P. C., Alfaro, M. E., Bolnick, D. I. and Hulsey, C. D. (2005). Many-to-One Mapping of Form to Function: A General Principle in Organismal Design? *Integr. Comp. Biol.* **45,** 256-262.

West, M., Slomianka, L. and Gundersen, H. J. G. (1991). Unbiased stereological estimation of the total number of neurons in the subdivisions of the rat hippocampus using the optical fractionator. *Anat. Rec.* **231,** 482-497.

Williams, R. W. and Herrup, K. (1988). The control of neuron number. *Annu. Rev. Neurosci.* **11,** 423-453.

Yang, G. C., Scherer, P. W. and Mozell, M. M. (2007a). Modeling Inspiratory and Expiratory Steady-State Velocity Fields in the Sprague-Dawley Rat Nasal Cavity. *Chem. Senses* **32,** 215-223.

Yang, G. C., Scherer, P. W., Zhao, K. and Mozell, M. M. (2007b). Numerical Modeling of Odorant Uptake in the Rat Nasal Cavity. *Chem. Senses* **32,** 273-284.

Youngentob, S. L., Mozell, M. M., Sheehe, P. R. and Hornung, D. E. (1987). A quantitative analysis of sniffing strategies in rats performing odor detection tasks. *Physiol. Behav.* **41,** 59-69.

Zhao, K., Dalton, P., Yang, G. C. and Scherer, P. W. (2006). Numerical Modeling of Turbulent and Laminar Airflow and Odorant Transport during Sniffing in the Human and Rat Nose. *Chem. Senses* **31,** 107-118.